

A Tsunami Forecast Model for Charlotte Amalie, VI

Elena Tolkova

Contents

1	Background and objectives	4
2	Forecast Methodology	5
3	Model Development	5
3.1	Forecast Area	6
3.2	Model Setup	6
3.2.1	Bathymetry sources	6
3.2.2	Grid selection	7
4	Results and Discussion	9
4.1	Model Validation using Saint Thomas Harbor resonance properties	9
4.2	Model Stability	10
5	Summary and Conclusion	11
6	Acknowledgments	12
A	Model *.in files for Charlotte Amalie, VI	13
A.1	Forecast model *.in file, to be used with MOST v.2	13
A.2	Reference and optimized model parameters in individual grids, to be used with MOST v.4	14
B	Propagation Database: Atlantic Ocean Unit Sources	42
C	SIFT Testing	52
C.1	PURPOSE	52
C.2	TESTING PROCEDURE	52
C.3	Results	53

List of Figures

1	Perspective view of the sea floor of the Atlantic Ocean and the Caribbean Sea. The Lesser Antilles are on the lower left side of the view, Florida is on the upper right, the Puerto Rico trench (purple) is at the center. Courtesy of the U.S. Geological Survey.	16
---	---	----

2	Saint Thomas harbor and the city of Charlotte Amalie, VI. Photo by Steve Frenkel.	17
3	Contours of grid A reference (red), A optimized (orange) and B (green, same extent for the both models); black 'x' - tide gauge. Colorscale - meters.	18
4	Grids B and C (same extent for the reference and forecast models). Two islands within C grid are Water island (the larger) and Hassel island (the smaller). Red 'x' points tide gauge location in Saint Thomas harbor. Colorscale - meters.	19
5	Boundary input into a B grid from reference (left pane) and optimized (right pane) A grids at 20 s and 45 s resolution. Y-axis: hour, X-axis: node along the B-boundary, colorscale: meters. Dashed vertical lines separate Western, Southern, Eastern, and Northern B-grid boundaries, followed counter-clock-wise. Crosses mark the locations of the nodes where sample boundary time-series were taken from. Grid-test event.	20
6	B-boundary sample time-series at nodes shown with black 'x' in Figure 5 computed with the reference (black) and optimized (red) A-grids. Grid-test event.	21
7	Boundary inputs into optimized C grid directly from the optimized A grid (left pane), and with the use of intermediate B grid at 12 s (center pane) and 4 s (right pane) resolution. Y-axis: hour, X-axis: node along the C-boundary, colorscale: meters. Shown is wet section of the boundary only. Dashed vertical lines separate Southern boundary from the Western on the left and Eastern on the right. Crosses mark the locations of the nodes where sample boundary time-series were taken. Grid-test event.	22
8	C-boundary sample time-series at nodes shown with black 'x' in Figure 7 obtained directly from the reference A grid (red) and with the use of intermediate B grid at 12 s (blue) and 4 s (green) resolution. Grid-test event.	23
9	Top: Time histories at the gage computed with optimized A and B grids (blue), and further refined with the use of C grid at 2 s (red) and 0.667 s (black) resolution. Bottom: Time histories at the gage computed with the reference (black) and optimized (red) set of grids. Grid-test event.	24
10	Synthetic mega event origins in the Caribbean: dots represent unit sources for Mega 1 event (red), Mega 2 (cyan), Mega 3 (green), Mega 4 (blue), Mega 5 (magenta). Red star - Virgin Islands model area.	25
11	Mega 1 event. Time histories at the gage location (top) and another observation point, according to Forecast Model (red) and Reference Model (black).	26
12	Same as above, for Mega 2 event.	27
13	Same as above, for Mega 3 event.	28
14	Same as above, for Mega 4 event.	29
15	Same as above, for Mega 5 event.	30
16	Same as above, for Mega 6 event.	31
17	Maximum water elevation with respect to still sea level within B grid, according to Forecast Model (right) and Reference model (left) for Mega 1 event. X-axis: longitude, degree East, Y-axis - latitude, degree North. Colorscale: cm.	32
18	Maximum water elevation with respect to still sea level within C grid, according to Forecast Model (right) and Reference model (left) for Mega 1 event. X-axis: longitude, degree East, Y-axis - latitude, degree North. Colorscale: cm. Crosses: observation points.	33
19	Same as above for Mega 2 event in B grid.	33
20	Same as above for Mega 2 event in C grid.	34
21	Same as above for Mega 3 event in B grid.	34

22	Same as above for Mega 3 event in C grid.	35
23	Same as above for Mega 5 event in B grid.	35
24	Same as above for Mega 5 event in C grid.	36
25	Area inundated by mega tsunamis (event Mega 1 (top left), Mega 2 (top right), Mega 3 (bottom left), and Mega 5 (bottom right)), according to Forecast Model. Only originally dry land is shown, with inundated area shown in blue. Colorscale - meters (does not apply to the inundated area).	37
26	Saint Thomas Harbor gauge sample record (top), segment of the de-tided record (bottom). Time since 00:00 Aug. 1, 2011.	38
27	Power spectrum of Saint Thomas Harbor gauge background signal (black) and five-event-averaged power spectrum of the first EOF mode time history (red).	39
28	Concatenated fragments of the five simulated tsunamis in a sample node in the harbor, since 310 min from the start of each simulation in grid C. The boundary input into the grid was terminated at 300 min. Each event data set was normalized by its RMS value.	40
29	Distribution of the normal oscillation amplitude, as deduced from the amplitude of the first complex EOF mode of concatenated tsunami scenarios.	41
30	Atlantic Source Zone unit sources.	44
31	South Sandwich Islands Subduction Zone.	50
32	Response of the Charlotte Amalie forecast model to synthetic scenario ATSZ 38-47 (alpha=25). Maximum sea surface elevation for A-grid (top left), B-grid (top right), C-grid (center). Sea surface elevation time series at the C-grid warning point (bottom), to be compared with the red curve in Figure 11, top pane.	55
33	Response of the Charlotte Amalie forecast model to synthetic scenario ATSZ 48-57 (alpha=25). Maximum sea surface elevation for A-grid (top left), B-grid (top right), C-grid (center). Sea surface elevation time series at the C-grid warning point (bottom), to be compared with the red curve in Figure 12, top pane.	56
34	Response of the Charlotte Amalie forecast model to synthetic scenario SSSZ 1-10 (alpha=25). Maximum sea surface elevation for A-grid (top left), B-grid (top right), C-grid (center). Sea surface elevation time series at the C-grid warning point (bottom), to be compared with the red curve in Figure 16, top pane.	57

List of Tables

1	Parameters of the reference and optimized grids. Run times correspond for 10-hour-long simulation.	7
2	Synthetic scenarios used with the model development and validation.	10
3	Maximum run-up heights in C grid according to Reference Model and Forecast Model.	11
4	Forecast model parameter file for optimized 10-hour simulation with MOST v.2.	13
5	Reference model parameter file for 10-hour simulation with MOST v.2.	14
6	Parameters for reference and optimized 10-hour simulation with MOST v.4. Each grid has a specific set of the parameters.	15
7	Earthquake parameters for Atlantic Source Zone unit sources.	45
8	Earthquake parameters for South Sandwich Islands Subduction Zone unit sources.	51
9	Table of maximum and minimum amplitudes at Charlotte Amalie, Virgin Islands warning point for synthetic and historical events tested using SIFT.	54

Abstract

Based on Method Of Splitting Tsunami (MOST) numerical model, a tsunami Forecast Model has been developed for a city of Charlotte Amalie, VI, centered on St. Thomas harbor, along with a reference inundation model at higher resolution and larger spatial coverage. Both models showed robust performance with a number of synthetic events, including extreme scenarios. Simulations of several tsunami events with the Forecast Model and with the Reference Model are performed and analyzed for the models validation and for the associated hazard evaluation. It is expected, that the forecast model for Charlotte Amalie, VI is able to provide an accurate estimate of a wave arrival time, wave height, and inundation extend in minutes of computational time in advance of a tsunami arrival, should the tsunami happen.

1 Background and objectives

The National Oceanic and Atmospheric Administration (NOAA) Center for Tsunami, Research (NCTR) at the NOAA Pacific Marine Environmental Laboratory (PMEL) has developed a tsunami forecasting capability for operational use by NOAA's two Tsunami Warning Centers located in Hawaii and Alaska (Titov et al., 2005). The system is designed to efficiently provide basin-wide warning of approaching tsunami waves accurately and quickly. The system, termed Short-term Inundation Forecast of Tsunamis (SIFT), combines real-time tsunami event data with numerical models to produce estimates of tsunami wave arrival times and amplitudes at a coastal community of interest. The SIFT system integrates several key components: deep-ocean observations of tsunamis in real time, a basin-wide pre-computed propagation database of water level and flow velocities based on potential seismic unit sources, an inversion algorithm to refine the tsunami source based on deep-ocean observations during an event, and high-resolution tsunami forecast models.

The Virgin Islands are a group of islands in the Caribbean, about 40 miles (64 km) east of Puerto Rico. The Virgin Island archipelago is made up of United States and British territories. The U.S. Virgin Islands consists of the main islands of St. Thomas, St. John, St. Croix and many smaller surrounding islands. The total land area of the territory is 133.73 square miles (346.4 sq. km).

The city of Charlotte Amalie is the territorial capital and the largest city of the U.S. Virgin Islands. It is located on the island of Saint Thomas and as of 2000 had an estimated population of 18,914, while the population of Saint Thomas was 51,181, or about 47% of the US Virgin Islands total (Census, 2000). The city is also a popular vacation destination, so the visitors add to the population significantly. Charlotte Amalie is famous as a deep-water harbor (see Figure 2), that was once a haven for pirates and is now one of the most popular cruise ports in the Caribbean, with about 1.5 million cruise ship passengers landing there each year.

At the same time, the region is at risk for far-field tsunamis that originate from earthquakes across the Atlantic; local earthquakes on the Caribbean subduction zone; and local landslides. The region is believed to be hit by two tsunamis which came from shores of Portugal in 1755 and in 1761 (Grothe et al., 2010). The examples of the region's high seismicity include a magnitude 7.5 earthquake centered northwest of Puerto Rico in 1943, and magnitude 8.1 and 6.9 earthquakes north of Hispaniola in 1946 and 1953, respectively. Some earthquakes generated tsunamis. Immediately after the 1946 earthquake, a tsunami struck northeastern Hispaniola and moved inland for several kilometers. Some reports indicate that nearly 1,800 people drowned. A 1918 magnitude 7.5 earthquake resulted in a tsunami that killed at least 40 people in northwestern Puerto

Rico. Eyewitness reports of an 1867 Virgin Islands tsunami gave a maximum wave height of more than 7 m in Frederiksted, St. Croix, where a large naval vessel was left on top of a pier (<http://woodshole.er.usgs.gov/project-pages/caribbean/>).

Based on Method Of Splitting Tsunami (MOST) numerical model, a tsunami Forecast Model has been developed for a city of Charlotte Amalie, VI, centered on St. Thomas harbor. The objective of this report is to describe the development of the operational tsunami forecast model for Charlotte Amalie, VI.

2 Forecast Methodology

The NOAA tsunami forecast system employs the Method of Splitting Tsunami (MOST) numerical model (Titov & Synolakis , 1998), which is a set of code for simulating three processes of tsunami evolution: generation by an earthquake, transoceanic propagation, and inundation of dry land at specific sites.

The forecast is supported by the database of an ocean-wide 36-hour-long simulation of a tsunami wave propagation, for numerous tsunamis generated by hypothetical unit earthquakes covering worldwide subduction zones (Gica et al., 2008). As the tsunami wave propagates across the ocean and reaches tsunameter observation sites, the forecasting system uses a data inversion technique coupled with a pre-computed tsunami generation scenarios to deduce the tsunami source in terms of the database unit earthquakes (Percival et al., 2009). A linear combination of the pre-computed unit tsunamis is then used to determine the offshore tsunami waves and to produce synthetic boundary conditions of water elevation and flow velocities into site-specific forecast models. The main objective of a forecast model is to provide an accurate estimate of a wave arrival time, wave height, and inundation extend at a particular location in minutes of computational time, in advance of the wave arrival. Previous and present development of forecast models in the Pacific (Titov et al., 2005; Titov, 2009; Tang et al., 2008; Wei et al., 2008) have validated the accuracy and efficiency of each forecast model currently implemented in the real-time tsunami forecast system.

3 Model Development

Each forecast model consists of three nested grids with increasing spatial resolution, referred to as A, B, and C-grids. The outer, coarser, grid A receives its boundary input of water elevation and flow velocities from the pre-computed database, and provides the boundary input of a re-fined (with respect to the database) solution into B grid, which is smaller in extent and finer in resolution. B grid's further refined solution provides the boundary input into the, finest and smallest of the grids, C grid. Within C grid, the solution is expected to be accurate enough to match the major features of a tide gauge tsunami record.

All tsunami forecast models are run in real time while a tsunami is propagating across the open ocean. Thus the computational time is the critical factor for a model development. Meeting the time constrain is achieved by manipulating with the spatial and temporal resolution of grids used in modeling, with an objective to balance computational speed with numerical accuracy.

The development of a Forecast Model is centered around "optimizing" (reducing) coverage and resolution of computational grids, to reduce the computational time as much as possible without

noticeable degradation of the numerical solution, in particular, a time history at an observational point (usually, at a tide gage location). Time histories computed with optimized grids are evaluated by visual comparison with the time history obtained with a reference model comprised of larger and/or finer grids (Tang et al., 2009).

3.1 Forecast Area

As provided by the U.S. Geological Survey (<http://woodshole.er.usgs.gov/project-pages/caribbean/>), Puerto Rico, the Virgin Islands to its east, and eastern Hispaniola to its west, are located on an active plate boundary zone between the North American plate and the northeast corner of the Caribbean plate, as shown in Figure 1, courtesy of USGS. The Caribbean plate slides eastward at about 2 cm/yr relative to the North American plate with a small component of subduction (one plate sinks under the other plate). In contrast, the Caribbean plate farther east overrides the North American plate, creating the island arc of the Lesser Antilles with its active volcanoes. There are no active volcanoes in Virgin Islands, though most of the islands, including Saint Thomas, are volcanic in origin.

Because Puerto Rico and Virgin Islands are located at an active plate boundary, earthquakes are a constant threat, and the densely populated coastal areas are vulnerable to tsunamis. The U.S. Geological Survey points out that all of the known causes of tsunamis are present in the Caribbean – earthquakes, submarine landslides, submarine volcanic eruptions, as well as trans-oceanic tsunamis from distant sources.

This work aims on forecasting possible future tsunamis approaching the city of Charlotte Amalie, the territorial capital and the largest city of the U.S. Virgin Islands located on the island of Saint Thomas.

The area's tide gage is located in Saint Thomas Harbor, at $18.335000^{\circ}\text{N}$, $64.920000^{\circ}\text{W}$. The tide station in the area was established in Jan 27, 1975, and the present installation since Feb 23, 1991. The gage location on a map is shown in Figure 4. There is no instrumental record of any of the historical tsunamis in this area.

3.2 Model Setup

3.2.1 Bathymetry sources

The forecast model A-grid was cut from Gulf Coast / Caribbean grid with 9 arc-sec resolution, merged with Virgin Islands DEM with 1 arc-sec resolution. The first data set was compiled from a variety of sources (NGDC, 2005), with occasional visible mismatch between the corresponding areas. Smoothing was performed along the mismatching area boundaries. There was no conversion to a common vertical datum among the sources, which yields Mean Sea Level as the assumed vertical reference for the first grid. The grid contains no topography data. The data in shallow areas around Virgin Island greatly mismatch the data for the same location in U.S. Virgin Islands 1 arc-sec grid. The later appear to be more realistic, so the two data sets were merged together, with the 9-sec data used in the deeper water where 1-sec data were not available.

B grid was cut from Virgin Islands DEM with 1 arc-sec resolution, and C grid was cut from St. Thomas and St. John DEM with 1/3 arc-sec resolution, both DEMs being referenced to Mean High Water, for modeling of worst-case scenario flooding (Grothe et al., 2010).

Grid name	spacing, arc-s		row×clm	dt_{max} , s	dt , s	CPU time, min	total, min
	(lat)	(lon)					
A ref	20	21	1614 × 523	2.31	2.0	91.7	108 (v.4)
B ref	4	4	420 × 251	6.0	4.0	5.4	115 (v.2)
C ref	0.67	0.67	351 × 226	1.17	1.0	10.9	
A opt	45	47.2	610 × 197	5.2	5.0	5.2	6 (v.4)
B opt	12	12	140 × 84	14.3	10.0	0.23	7 (v.2)
C opt	2	2	117 × 76	3.5	2.5	0.5	

Table 1: Parameters of the reference and optimized grids. Run times correspond for 10-hour-long simulation.

The later DEM was low-pass filtered to avoid aliasing when re-sampled to desired resolution. To ensure stability in simulations, all the grids were processed for SSL (Support Scientist’s Limit) which restricted variation of the refraction index between any two neighboring nodes to 2.1 times in B and C grids, and 1.9 in A grid (Tolkova, 2013).

The parameters of the reference and optimized grids are given in Table 1, and the grids’ coverage is shown in Figures 3, 4. Computational (CPU) times listed in the Table and anywhere in this work were recorded with Dell PowerEdge R510 Linux machine, 2 x 2.93 GHz Xeon E5670 hex-core processors, running MOST code compiled with PGI Fortran compiler.

Run times listed in Table 1 correspond for 10-hour-long simulation after a tsunami entered A grid. Run times in individual grids are obtained with MOST v.4, without using its option to parallelize computations. The last column shows the total duration of the entire 10-hour simulation in either set of grids, depending on the MOST version.

3.2.2 Grid selection

Experiments with different grids showed that within a reasonable range of resolutions, the model solution is mostly affected by the outer (A) grid coverage. Due to islands and underwater ridges acting as reflectors and waveguides, the wave energy gets redistributed toward later waves. To accurately simulate the amplitudes along the wave train, the outer grid should include the essential bathymetric/topographic features. In particular, for the test event, the waves arriving between 1 and 2.5 hour after the first arrival would be underestimated more than twice if an outer grid would not extend far enough to the West of PR to include the opposite piece of land, regardless of the grid resolution. The waves arriving during the next hour would be underestimated 2-3 times if the grid would not extend far enough South, to include underwater flats (see Figure 3). Being highly sensitive to the coverage of an A-grid, the model solution is not so with regard to B and C grids.

Reference A grid has a coverage of 2.9° (16.05°N to 18.95°N) x 9.4° (-69.9°E to -60.5°E), or 322.8 km x 996.8 km. Optimized A grid has a coverage of 2.45° (16.5°N to 18.95°N) x 8.0° (-69°E to -61°E), or 272.7 km x 848.3 km. The reference A grid has the finer resolution of 20 s of the Great arc, while the optimized A grid has a resolution of 45 s.

Reference and optimized versions of the B grid, as well as these versions of the C grid, have the same coverage determined by bathymetric/topographic feature. B grid has a coverage of 0.2767° (18.2217°N to 18.4983°N) x 0.4633° (-65.1500°E to -64.6867°E), or 30.80 km x 48.95 km. The reference B grid has a spacing of 4 s in both longitude and latitude, while the optimized B grid has

a spacing of 12 s.

C grid has a coverage of 0.0417° (18.3033°N to 18.3450°N) \times 0.0645° (-64.9704°E to -64.9059°E), or 4.638 km \times 6.811 km. The reference C grid has a spacing of 0.667 s in both longitude and latitude, while the optimized C grid has a spacing of 2 s.

To assist with and to justify the grid selection, the Forecast Model development was carried out with MOST version 4, rather than with the current operational version (v.2). The version 4 performs computations in one grid at a time and saves the boundary input time-series along the perimeter of each next-level grid (Tolkova, 2013). Thus a developer can observe how input into the next level grid depends on parameters (coverage, resolution) of the parent grid, and to select parameters of one grid at a time.

Below, the grid selection is justified with an artificial Mw 8.5 event, originated with unit sources a44-46, b44-46 (Atlantic subduction zone) with a factor 5 (referred to as grid-test event). To illustrate how the solution in an intermediate (B) grid is affected by an A grid resolution, B-grid boundary inputs were computed with both A grids. Figure 5 displays boundary time series on the perimeter of B grid, followed counter-clock-wise from the North-West corner, computed with the reference and optimized A grids. Samples of individual time histories at four boundary nodes can be found in Figure 6. It can be seen by visual comparison of the results, that the optimized A grid reproduces the wave train correctly in general in 18 times less of computational time, though with some loss of energy carried by the shorter waves.

Within the forecast methodology, a purpose of a B grid is to refine an A-grid solution before it goes into a C grid. Thus a C-grid input obtained directly from an A-grid provides the starting point from which refinements are to be made. To visualize those refinements and select a B grid resolution, boundary inputs into C grid were compared, computed directly from optimized A grid, and with the consequent use of either reference or optimized B grid (see Figure 7). It can be seen in time histories at selected points on C-grid boundary (see Figure 8), that additional scattering on near-shore features accounted for in B grid results in changes to the wave amplitude (earlier waves especially), though the general wave envelope as it comes from A grid is not much affected. The results for the two B grids of different resolution are practically identical, while the computations with the coarser grid are 23.4 times faster.

Similarly, a purpose of a C grid is to refine a B-grid solution for a locality. Thus a B-grid solution provides the starting point from which refinements are to be made. Figure 9, top pane, displays time histories at an observational point obtained directly from the optimized B-grid and further refined with the use of either reference or optimized C grid. The actual location of the nodes where the two C-grid time series were read from is 22 m apart from each other. The gage location in the B-grid coincides with its location in the reference C grid. It can be seen, that even B-grid solution provides a time history estimate fairly close to the most refined one (obtained with the finer C-grid), at least for the grid-test event. Time histories obtained with the two C grids are very close, with the computation time being 0.5 min for the coarser grid and 10.9 min for the finer grid. Finally, the time histories at the gage were computed with the set of the three reference grids and the three optimized grids (Figure 9, bottom pane). The 10 h simulation in the reference model takes 108 min of computer time with MOST v.4 and 115 min with the v.2. The 10 h simulation in the optimized model takes 6 min of computer time with MOST v.4 and 7 min with the v.2. The two sets of grids provide fairly close solutions, which verifies the optimized grids.

The models' parameter files are given in Appendix.

4 Results and Discussion

In the next section, the simulations of several tsunami events with the Forecast Model and with the Reference Model are analyzed for the models validation and for the associated hazard assessment.

4.1 Model Validation using Saint Thomas Harbor resonance properties

There is no record of an actual tsunami event at the location, so the model can not be validated by simulating historical events and comparing recorded and synthetic time histories at the observation point. For an alternative form of validation, we compare Saint Thomas Harbor resonance frequencies deduced from tidal records and from tsunami simulations. The model's ability to reproduce normal oscillations of the harbor in agreement with the observations is interpreted as an indication of its ability to correctly reproduce the wave dynamics in the area.

Saint Thomas Harbor has a stationary tsunami-capable tide gauge with 1-min sampling rate maintained by National Ocean Service (NOS). Its sample record is shown in Figure 26. The record displays normal oscillations of the harbor atop tidal signal. To detect resonance frequencies in the background signal, a power spectrum of a de-tided gauge record for four days of August 1-4, 2011 was computed. Due to the original sampling rate, frequencies above the tidal range, but under 30 c/h, or periods from 2 min to 3 h, are of interest. The power spectrum (dimensionless) was estimated as an amplitude of the Discrete Fourier Transform of a central fragment of the record auto-correlation coefficient weighted with a raised cosine window (Hamming, 1998). The window effective width was 384 min, which limits the frequency resolution to 0.16 c/h though the DFT is computed with 0.08 c/h increment. The greatest peak in the spectrum occurs at 2.5 c/h (see Fig. 27). To interpret it as a possible resonance frequency of the harbor, some estimates follow. The average depth in the harbor is $h = 10$ m. The length of the harbor all the way along Hassle Island is $l = 2.3$ km at most. Rectangular-shaped resonator with those parameters has the lowest resonance frequency $\sqrt{gh}/4l=3.6$ c/h. Resonators of the same average size, but with different shapes and depth profiles, might have the fundamental frequency up to 1.5 times lower (Wilson, 1972). Thus the observed frequency of 2.5 c/h can be interpreted as the fundamental resonance frequency of the harbor.

Should tsunami waves in the area be modeled accurately, the numerical solution would display similar resonance behavior. Hereafter, analysis of the model for resonance properties follows the technique suggested in (Tolkova and Power, 2011). To reproduce free oscillations in Saint Thomas Harbor in a numerical solution, mega events 1-5 (see Table 2) were simulated with Forecast Model in grid C for 15 hours, while the boundary input into the grid was provided for the first 5 hours of simulation only. Figure 28 shows computed time histories in all the events at some arbitrary node inside the harbor, after the boundary forcing has been terminated. It can be seen, that all the time histories are represented by a decaying single-frequency time-series at approximately 2.7 cycle/hour.

For each event, segments of the time histories between 310 and 900 min from the start of the simulation were collected from 759 nodes located within the harbor and near its mouth. The events were concatenated along the time axis, as discussed in (Tolkova and Power, 2011). Complex Empirical Orthogonal Function analysis performed on the concatenated events data, attributed 96% of the data variance to the single mode, which can be identified as the lowest (filling/emptying the entire harbor) normal mode. Its shape, i.e. space distribution of the normal oscillation amplitude, is shown in Figure 29.

The power spectrum of the background signal of the gauge and the five-event-average power spectrum of the normal mode time history scaled to the same peak height are shown in Figure 27. Wider spectral line in the numerical solution is due to combine effects of:

- artificial shortening of the oscillation life span by starting a time-series at the peak of the signal
- less than perfect isolation of the normal mode (which would require more thorough and representative selection of tsunami scenarios (Tolkova and Power, 2011));
- consequently, power spectra of individual events are centered around slightly different peak frequencies, so averaging results in widening of the peak;
- numerical dissipation.

The frequency of harbor oscillations in the numerical solution differ by only 8% from the frequency dominating the gauge background spectrum. The favorable comparison between the model resonance frequency and that found on the tide gauge acts as a validation of the tsunami model.

4.2 Model Stability

To infer on the tsunami behavior and the extent of associated danger, and also to test the Forecast and Reference Models for stability and for mutual consistence, a number of artificial events, including a micro-tsunami and six mega-tsunamis of Mw 9.3 were simulated for 30-36 h with both Models. The events sources were selected to represent different locations within Atlantic (Caribbean) subduction zone, namely AB38-47 (Mega 1), AB48-57 (Mega 2), AB58-67 (Mega 3), AB68-77 (Mega 4), AB82-91 (Mega 5), and South Sandwich subduction zone AB1-10 (Mega 6), and B11 (micro) (Gica et al., 2008). For the mega-events, the slip of 25 m was distributed evenly among the unit sources. Locations of the unit sources comprising the events in Caribbean basin are shown in Figure 10. Synthetic scenarios used for the model development and validation are listed in Table 2. In all the events, the solutions by the Forecast Model and the Reference Model displayed stable behavior and agree fairly well with each other.

Sub. Zone	Sources	Slip factor	Mw	name
Caribbean	ab38-47	25	9.3	Mega 1
Caribbean	ab48-57	25	9.3	Mega 2
Caribbean	ab58-67	25	9.3	Mega 3
Caribbean	ab68-77	25	9.3	Mega 4
Caribbean	ab82-91	25	9.3	Mega 5
S.Sandwich	ab1-10	25	9.3	Mega 6
S.Sandwich	b11	0.1	6.8	micro
Caribbean	b52	1	7.5	
Caribbean	ab44-46	5	8.5	grid-test

Table 2: Synthetic scenarios used with the model development and validation.

Comparison of the results by the two models for the mega-events is presented below. Figures 11-16 show time histories at the tide gage location and at another observation point in the port

event	RM, m	FM, m
Mega 1	5.56	5.95
Mega 2	16.92	17.07
Mega 3	2.81	2.35
Mega 4	0.81	0.76
Mega 5	8.95	7.51
Mega 6	0.52	0.80

Table 3: Maximum run-up heights in C grid according to Reference Model and Forecast Model.

outside (West) of Saint Thomas Harbor, computed with Forecast Model in comparison with results by Reference Model (see Fig.18 for the locations of both observation points). Figures 17-24 show maximal water elevation with respect to still sea level in grids B and C for the four events (1-3 and 5) with the greater impact at the forecasted area, Forecast Model in comparison with Reference Model.

As expected, the most devastating tsunami Mega 2 originated in the immediate vicinity of the forecast area (see Fig. 10). The maximum run-up heights within C grid are summarized in Table 3.

Reference Model and Forecast Model solutions are very close for the Caribbean events, and for the first five hours since the arrival of the tsunami originated at South Sandwich Islands (Mega 6). In this last case, the major waves arrive at least somewhat 5 hours after the first wave arrival, and their amplitudes are over-estimated with the Forecast Model.

Mega events 1-3 and 5 with higher run-ups caused some inundation, with the most affected area being around Crown Bay, West of St.Thomas Harbor and just North of Water Island. Land areas in C grid inundated anytime within 30 h after the tsunami generation in those events are shown in Figure 25. The inundation was computed using Forecast Model.

5 Summary and Conclusion

A tsunami Forecast Model has been developed for an island of Charlotte Amalie, VI, centered on St. Thomas harbor. The model showed robust performance with a number of synthetic events, including extreme scenarios. In the absence of records of any actual tsunami at the location, the validity of the model is deduced from the following considerations:

- MOST numerical model has been proved to simulate tsunami propagation and run-up correctly for numerous locations and events throughout the Globe, subject to the accuracy of the numerical set-up;
- the proper choice of the numerical parameters for the Charlotte Amalie model (such as the model coverage, spatial and temporal resolution) was given full attention to, as described in detail in this report;
- the general wave patterns and time histories by the coast evaluated with the reference and the optimized models are consistent with each other;

- harbor oscillations in the numerical solution occur on the same frequency as found in the St. Thomas harbor gauge background spectrum.

Therefore it is expected, that the forecast model for the Charlotte Amalie, VI is able to provide an accurate estimate of a wave arrival time, wave height, and inundation extent in advance of a tsunami arrival, should the tsunami happen, subject to the accuracy of topography information. The 10 hour simulation of the tsunami propagation and run-up in the area presently requires 6-7 min of computational time (Dell Power-Edge Linux computer), depending on the MOST version employed.

The bathymetry and topography data used in the development of this forecast model are based on a digital elevation model provided by the National Geophysical Data Center. Photo evidence collected in the area gives reasons to believe, that low-lying near-shore areas, where major town activity happens, are present in current Forecast Model (based on the DEM provided) over-elevated up to 10 m. Thus inundation extent can be severely under-estimated. As new digital elevation models become available, forecast models will be updated and report updates will be posted at http://nctr.pmel.noaa.gov/forecast_reports/.

6 Acknowledgments

This study and publication is funded by the Joint Institute for the Study of the Atmosphere and Ocean (JISAO) under NOAA Cooperative Agreement No. ..., Contribution (JISAO), ... (PMEL).

References

- Gica E., Spillane M.C., Titov V.V., Chamberlin C.D. and Newman J.C. (2008): Development of the forecast propagation database for NOAA's Short-Term Inundation Forecast for Tsunamis (SIFT), NOAA Tech. Memo. OAR PMEL-139, 89pp.
- Grothe, P. et al. 2010. Digital Elevation Models of the U.S. Virgin Islands: Procedures, Data Sources and Analysis. NOAA National Geophysical Data Center (NGDC), 56 pp.
http://onda.pmel.noaa.gov/atlas/citation/171/st._croix_vi.pdf
- National Geophysical Data Center. East coast and Gulf Coast and Caribbean nine second tsunami propagation grids compilation report, 11 pp.
http://onda.pmel.noaa.gov/atlas/citation/10/9sec_intermediate_sub.doc
- Hamming RW (1998) Digital Filters. Dover publications, Inc. Mineola, New York
- Tang, L., V.V. Titov, Y. Wei, H.O. Mofjeld, M. Spillane, D. Arcas, E.N. Bernard, C. Chamberlin, E. Gica, and J. Newman (2008): Tsunami forecast analysis for the May 2006 Tonga tsunami. J. Geophys. Res., 113, C12015, doi: 10.1029/2008JC004922.
- Tang L., V. V. Titov, and C.D.Chamberlin (2009): Development, testing, and applications of site-specific tsunami inundation models for real-time forecasting. J. Geophys. Res., 114, C12025, doi: 10.1029/2009JC005476.

- Titov V. V., González F. I., Bernard E. N., Eble M. C., Mofjeld H. O., Newman J. C., Venturato A. J., 2005. Real - Time Tsunami Forecasting: Challenges and Solutions. *Natural Hazards*, 35: 41 - 58.
- Titov V. V., Synolakis C. E., Numerical Modeling of Tidal Wave Runup, 1998, *J. Waterway, Port, Coastal and Ocean Eng.*, V 124, July / August, N 4, 157 - 171.
- Titov, V.V., 2009. Tsunami forecasting. Chapter 12 in *The Sea, Volume 15: Tsunamis*, Harvard University Press, Cambridge, MA and London, England, 371400.
- Wei, Y., E. Bernard, L. Tang, R. Weiss, V. Titov, C. Moore, M. Spillane, M. Hopkins, and U. Kanoglu (2008): Real-time experimental forecast of the Peruvian tsunami of August 2007 for U.S. coastlines. *Geophys. Res. Lett.*, 35, L04609, doi: 10.1029/2007GL032250.
- E. Tolkova and W. Power (2011). Obtaining natural oscillatory modes of bays and harbors via Empirical Orthogonal Function analysis of tsunami wave fields. *Ocean Dynamics*, Vol.61/6, pp. 731-751. doi: 10.1007/s10236-011-0388-5
- E. Tolkova. Method of Splitting Tsunamis (MOST), version 4. In preparation.
- Wilson B (1972) Seiches. *Advances in Hydrosiences* 8:1-94
- The U.S. Geological Survey, Woods Hole. Caribbean Tsunami and Earthquake Hazards Studies. <http://woodshole.er.usgs.gov/project-pages/caribbean/>
- U.S. Census Bureau. <http://www.census.gov>

A Model *.in files for Charlotte Amalie, VI

A.1 Forecast model *.in file, to be used with MOST v.2

0.001	Minimum amp. of input offshore wave (m)
1.0	Minimum depth of offshore (m)
0.1	Dry land depth of inundation (m)
0.0009	Friction coefficient (n^{**2})
1	run up in a and b
300.0	max wave height meters
2.5	time step (sec)
14400	number of steps for 10 h simulation
2	Compute "A" arrays every n-th time step, n=
4	Compute "B" arrays every n-th time step, n=
12	Input number of steps between snapshots
0	...starting from
1	...saving grid every n-th node, n=

Table 4: Forecast model parameter file for optimized 10-hour simulation with MOST v.2.

0.001	Minimum amp. of input offshore wave (m)
1.0	Minimum depth of offshore (m)
0.1	Dry land depth of inundation (m)
0.0009	Friction coefficient (n^{**2})
1	run up in a and b
300.0	max wave height meters
1.0	time step (sec)
36000	number of steps for 10 h simulation
2	Compute "A" arrays every n-th time step, n=
4	Compute "B" arrays every n-th time step, n=
32	Input number of steps between snapshots
0	...starting from
1	...saving grid every n-th node, n=

Table 5: Reference model parameter file for 10-hour simulation with MOST v.2.

A.2 Reference and optimized model parameters in individual grids, to be used with MOST v.4

	A ref	B ref	C ref	A opt	B opt	C opt
Min ampl. of input wave (m)	0.001	0.001	0.001	0.001	0.001	0.001
Min depth offshore (m)	1	1	1	1	1	1
Dry land depth (m)	0.1	0.1	0.1	0.1	0.1	0.1
Friction coef. (n**2)	0.0009	0.0009	0.0009	0.0009	0.0009	0.0009
number of grids	2	2	1	2	2	1
outer interp	4	4	2	2	2	2
inner interp	4	4	2	2	2	2
grids	A ref, B ref	B ref, C ref	C ref	A opt, B opt	B opt, C opt	C opt
runup flag	1	1	2	1	1	2
time step (sec)	2	4	1	5	10	3
continue past input	0	0	0	0	0	0
amount of steps	18000	9000	36000	7200	3600	12000
steps between snapshots	30	15	30	12	6	20
saving inner bndr every n steps	2	1	1	1	1	1
saving every n-th node, n=	3	2	1	2	2	1

Table 6: Parameters for reference and optimized 10-hour simulation with MOST v.4. Each grid has a specific set of the parameters.

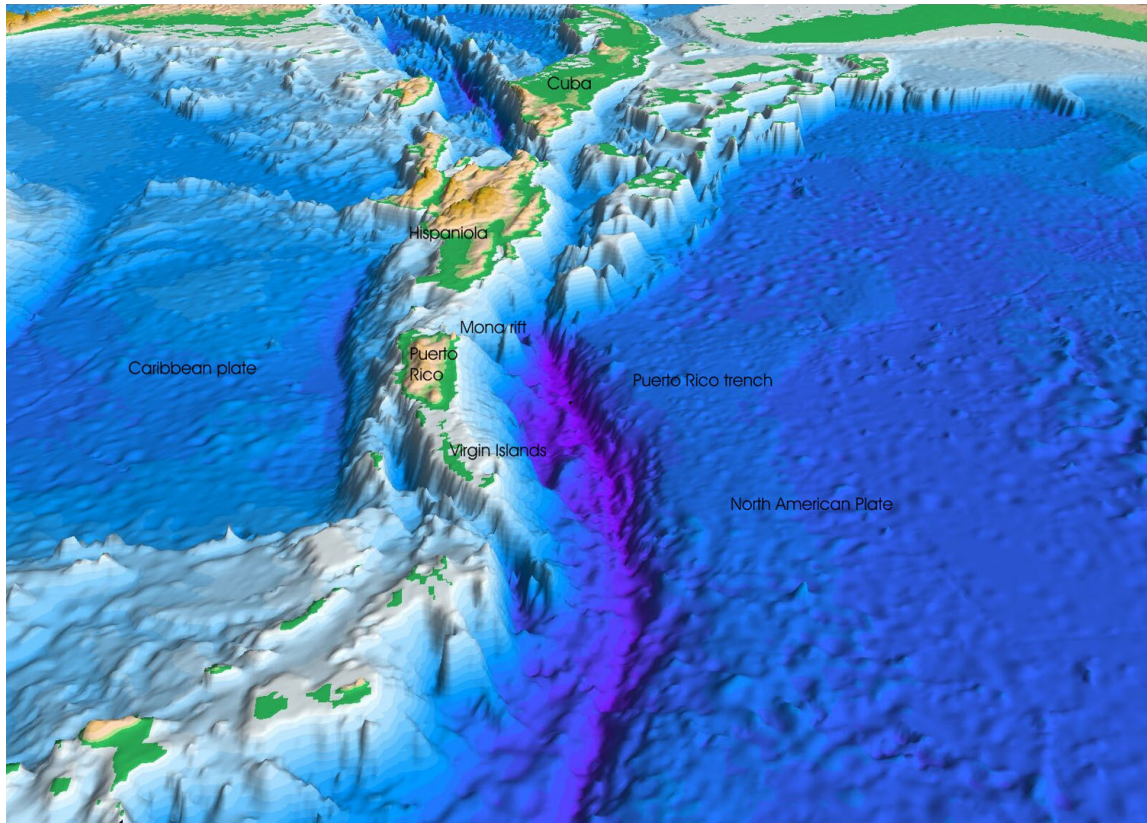


Figure 1: Perspective view of the sea floor of the Atlantic Ocean and the Caribbean Sea. The Lesser Antilles are on the lower left side of the view, Florida is on the upper right, the Puerto Rico trench (purple) is at the center. Courtesy of the U.S. Geological Survey.



Figure 2: Saint Thomas harbor and the city of Charlotte Amalie, VI. Photo by Steve Frenkel.

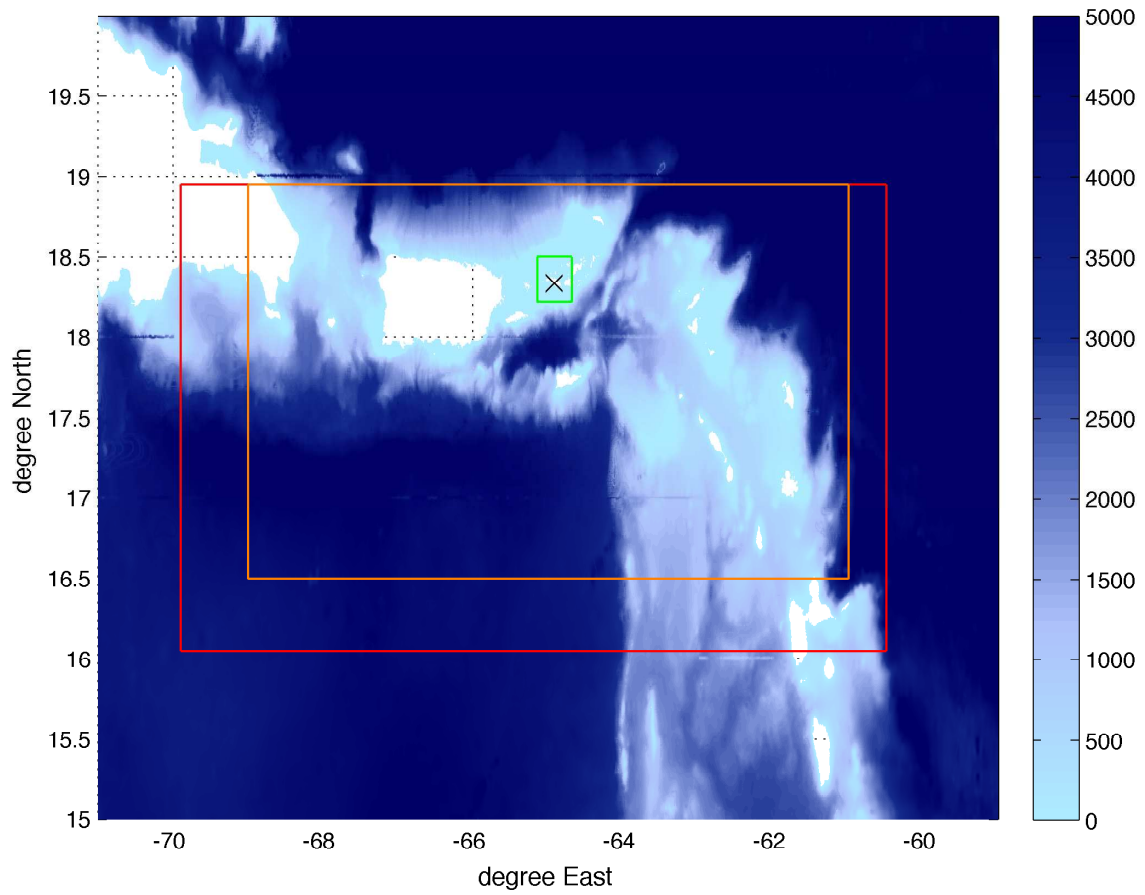


Figure 3: Contours of grid A reference (red), A optimized (orange) and B (green, same extent for the both models); black 'x' - tide gauge. Colorscale - meters.

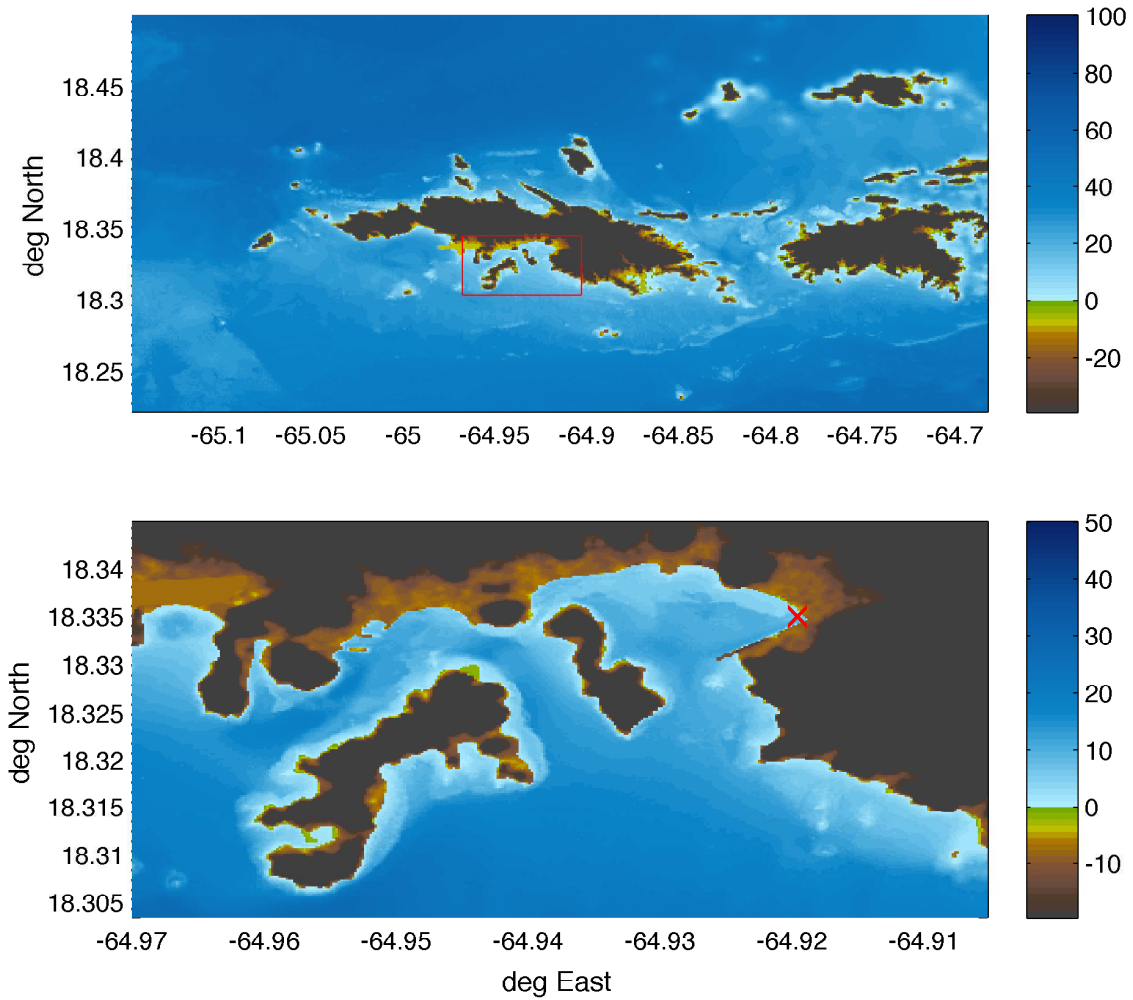


Figure 4: Grids B and C (same extent for the reference and forecast models). Two islands within C grid are Water island (the larger) and Hassel island (the smaller). Red 'x' points tide gauge location in Saint Thomas harbor. Colorscale - meters.

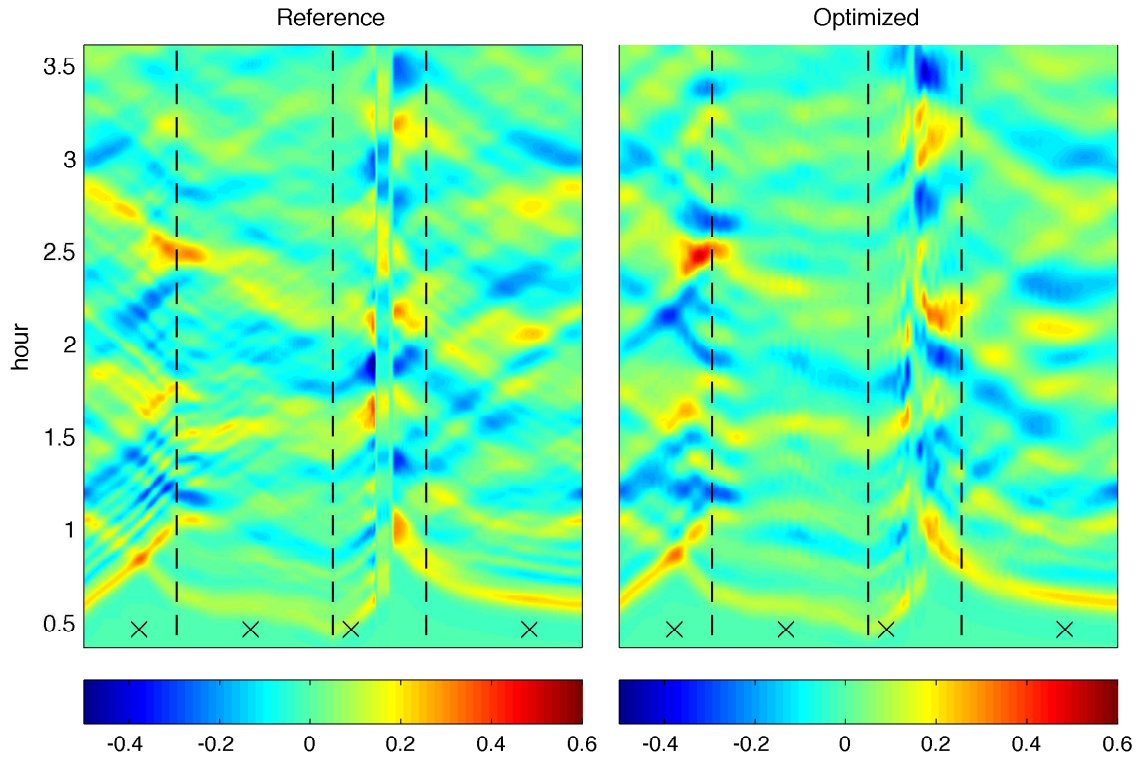


Figure 5: Boundary input into a B grid from reference (left pane) and optimized (right pane) A grids at 20 s and 45 s resolution. Y-axis: hour, X-axis: node along the B-boundary, colorscale: meters. Dashed vertical lines separate Western, Southern, Eastern, and Northern B-grid boundaries, followed counter-clock-wise. Crosses mark the locations of the nodes where sample boundary time-series were taken from. Grid-test event.

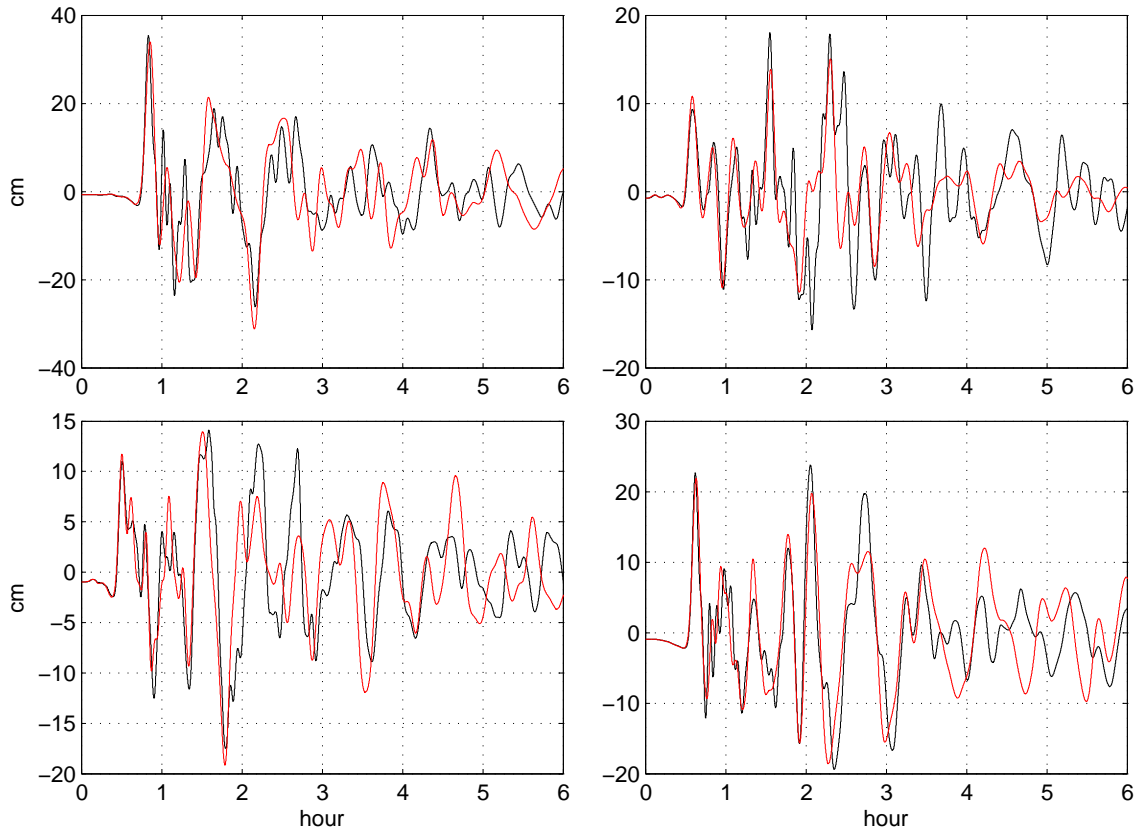


Figure 6: B-boundary sample time-series at nodes shown with black 'x' in Figure 5 computed with the reference (black) and optimized (red) A-grids. Grid-test event.

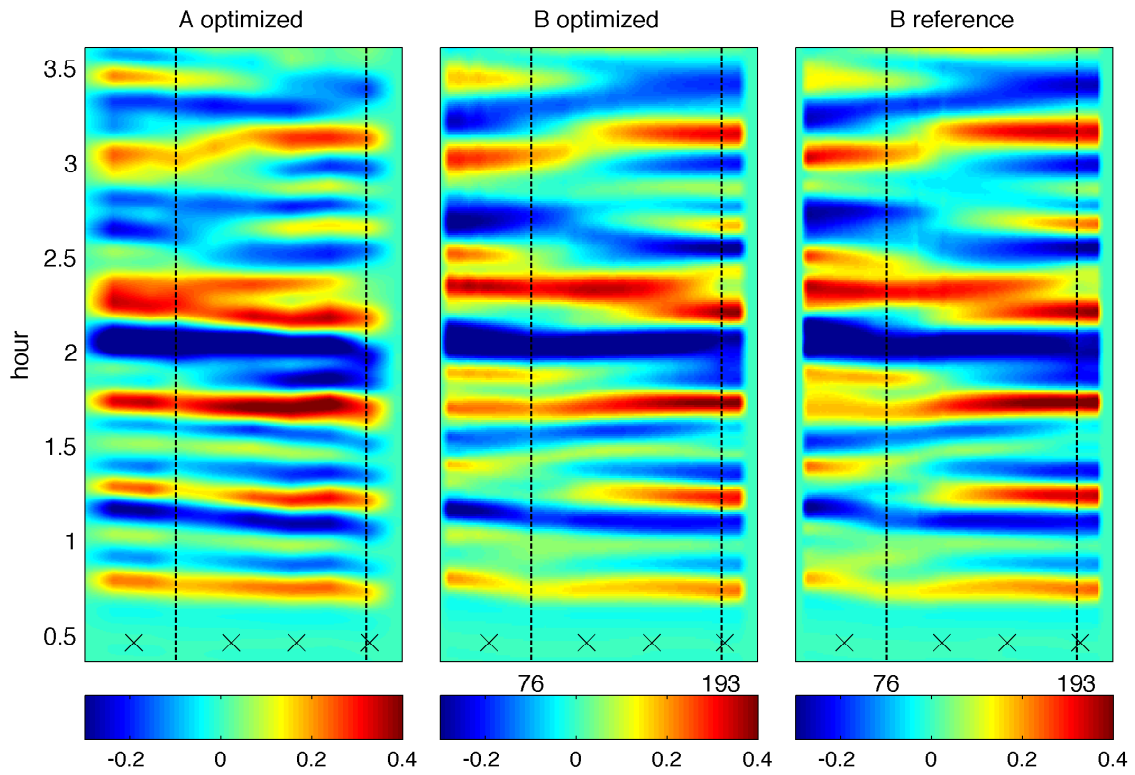


Figure 7: Boundary inputs into optimized C grid directly from the optimized A grid (left pane), and with the use of intermediate B grid at 12 s (center pane) and 4 s (right pane) resolution. Y-axis: hour, X-axis: node along the C-boundary, colorscale: meters. Shown is wet section of the boundary only. Dashed vertical lines separate Southern boundary from the Western on the left and Eastern on the right. Crosses mark the locations of the nodes where sample boundary time-series were taken. Grid-test event.

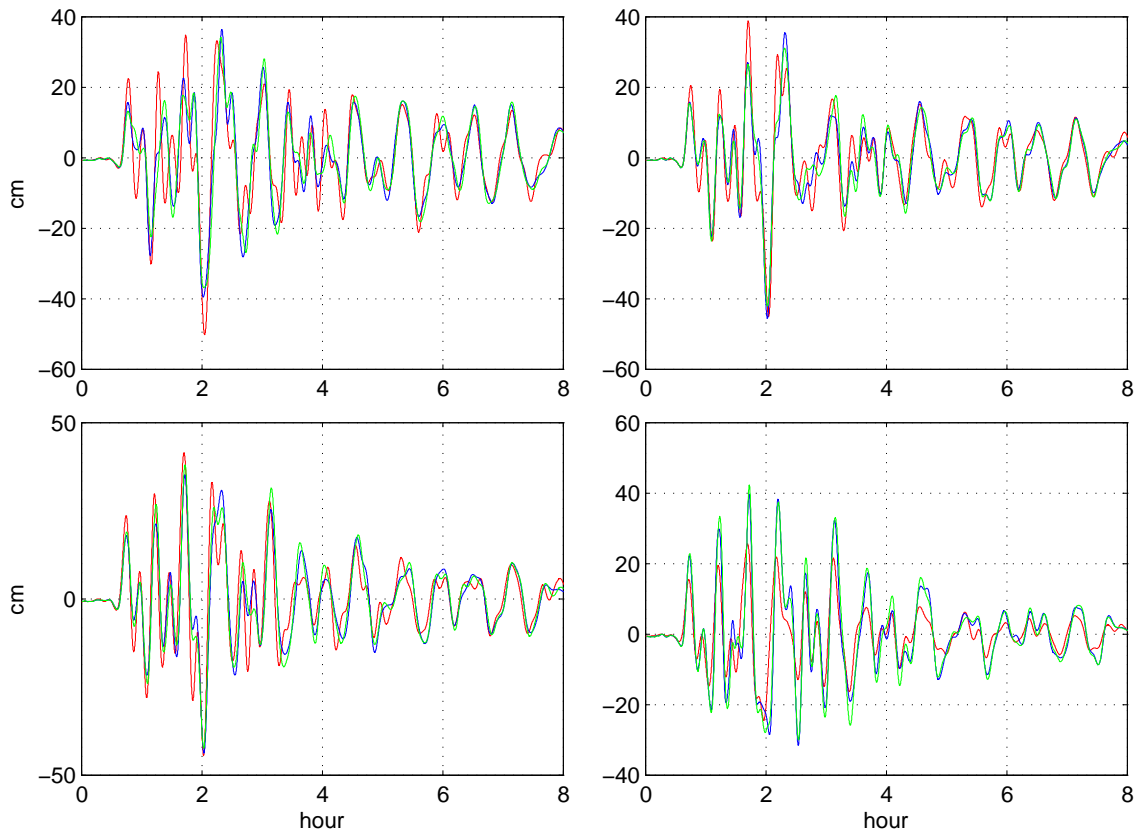


Figure 8: C-boundary sample time-series at nodes shown with black 'x' in Figure 7 obtained directly from the reference A grid (red) and with the use of intermediate B grid at 12 s (blue) and 4 s (green) resolution. Grid-test event.

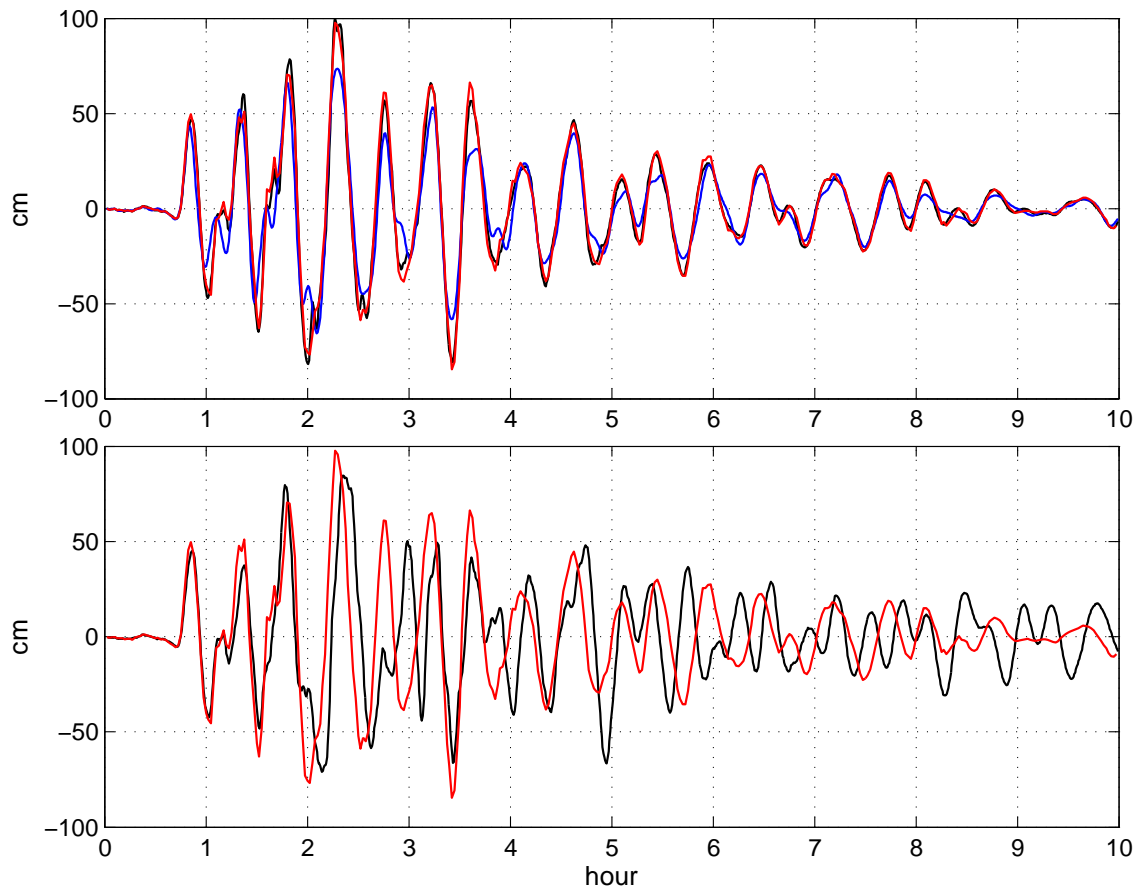


Figure 9: Top: Time histories at the gage computed with optimized A and B grids (blue), and further refined with the use of C grid at 2 s (red) and 0.667 s (black) resolution. Bottom: Time histories at the gage computed with the reference (black) and optimized (red) set of grids. Grid-test event.

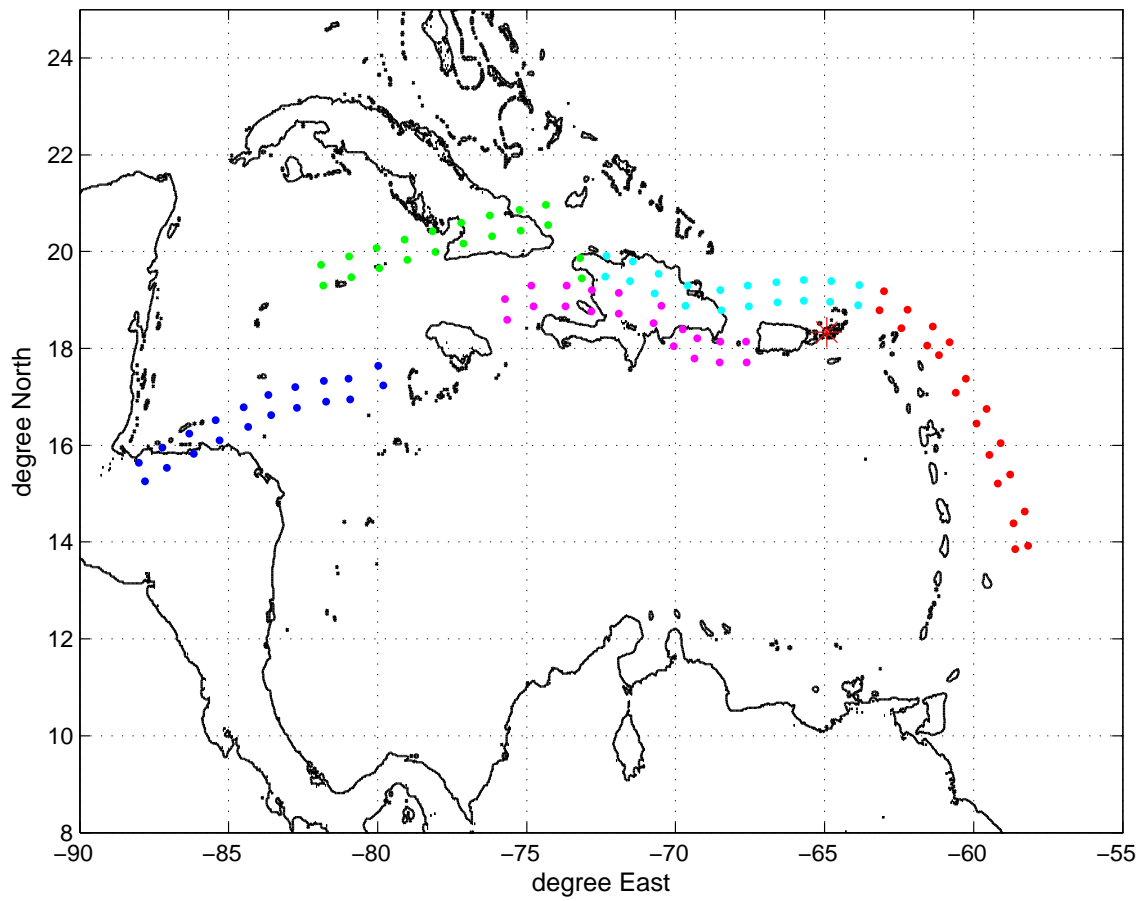


Figure 10: Synthetic mega event origins in the Caribbean: dots represent unit sources for Mega 1 event (red), Mega 2 (cyan), Mega 3 (green), Mega 4 (blue), Mega 5 (magenta). Red star - Virgin Islands model area.

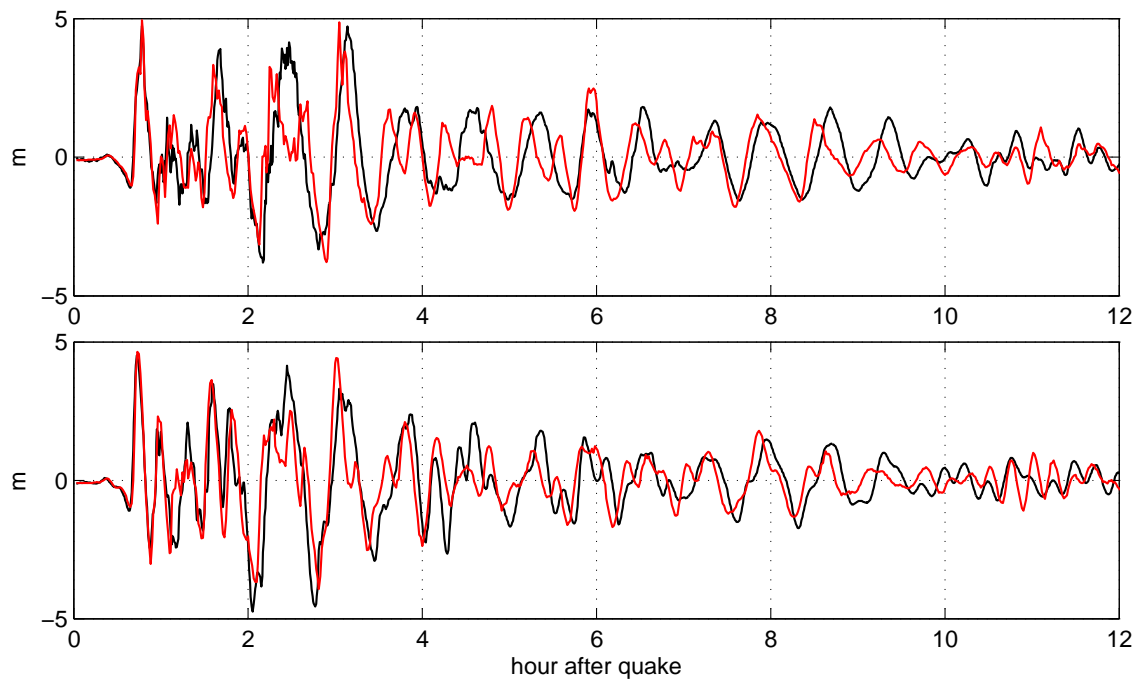


Figure 11: Mega 1 event. Time histories at the gage location (top) and another observation point, according to Forecast Model (red) and Reference Model (black).

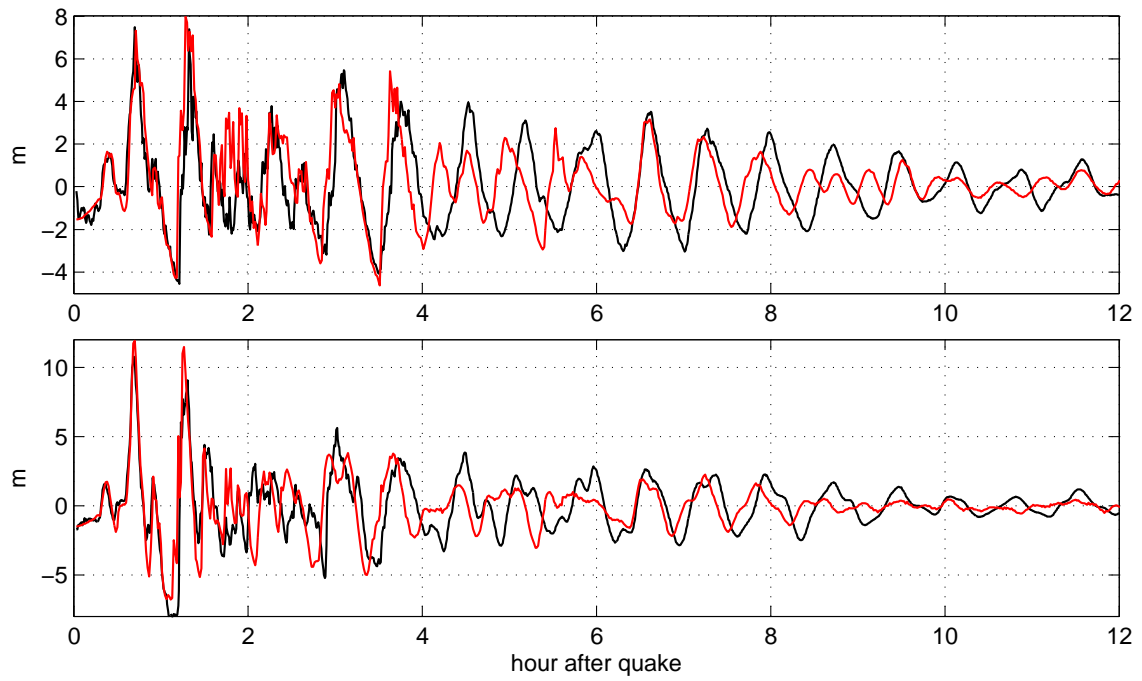


Figure 12: Same as above, for Mega 2 event.

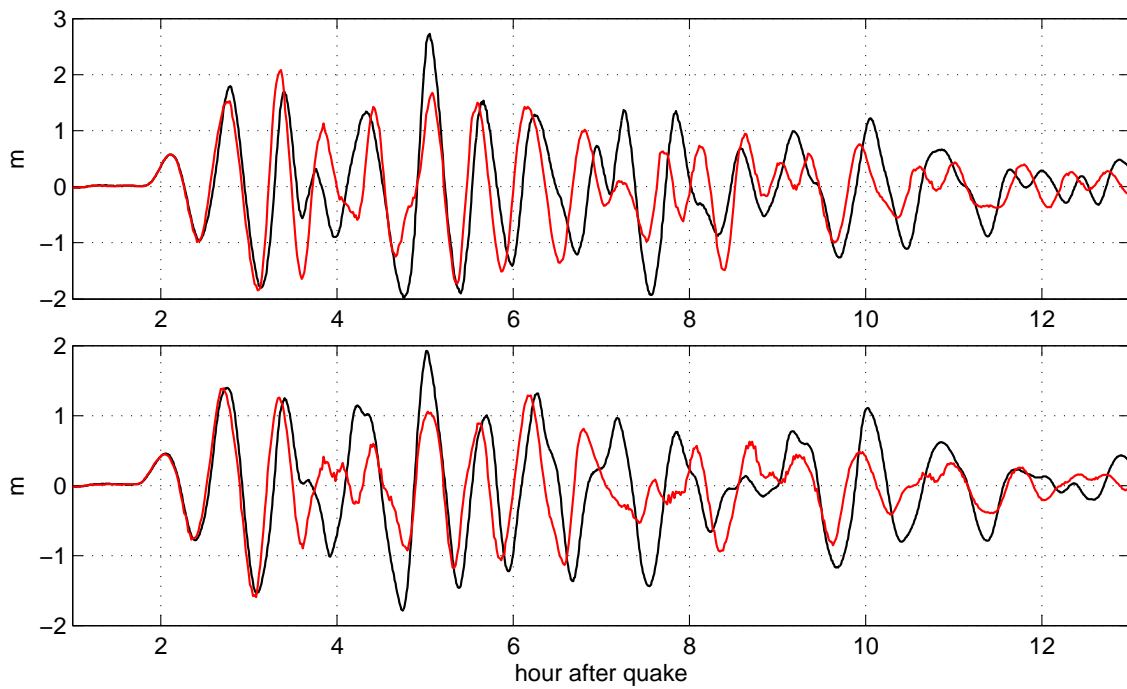


Figure 13: Same as above, for Mega 3 event.

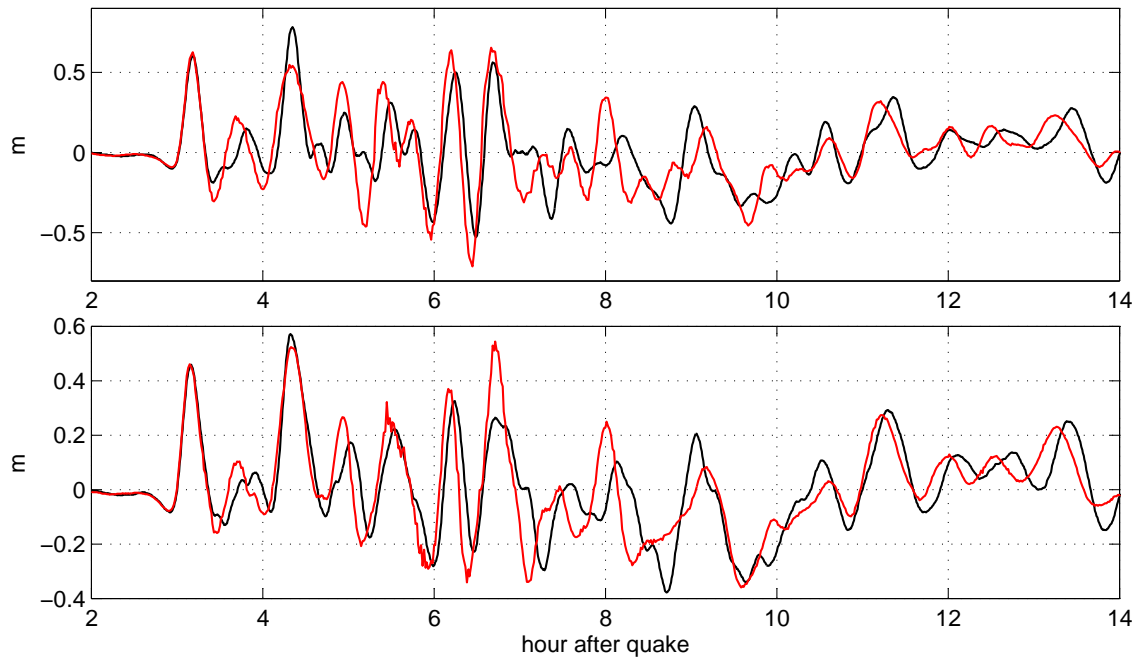


Figure 14: Same as above, for Mega 4 event.

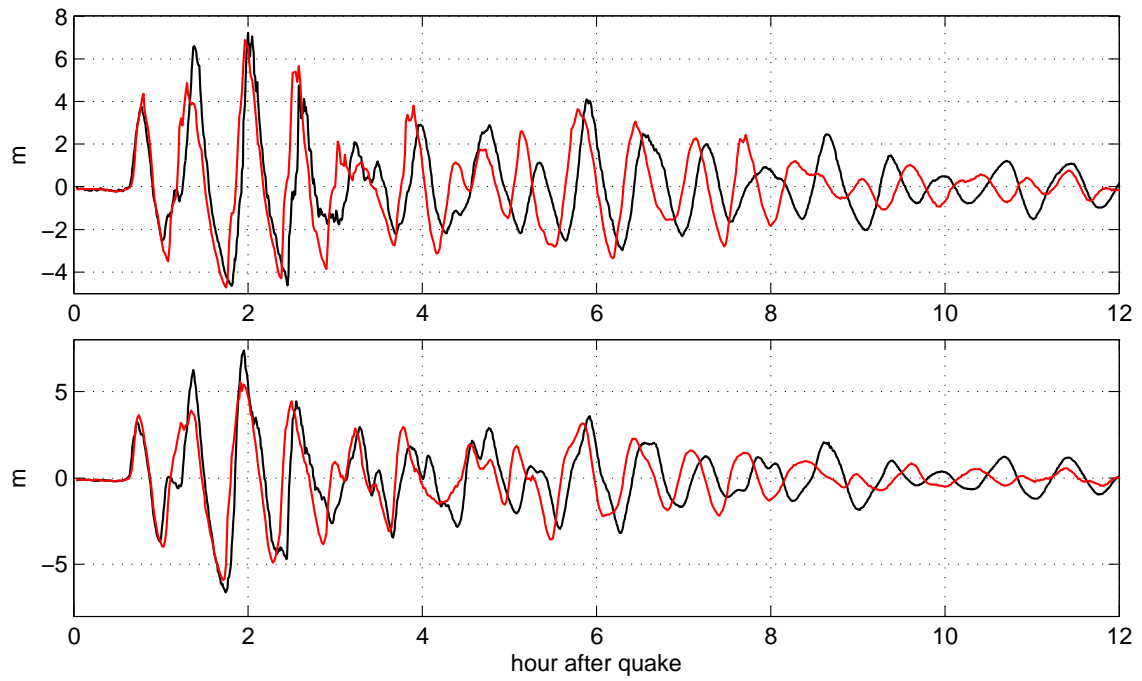


Figure 15: Same as above, for Mega 5 event.

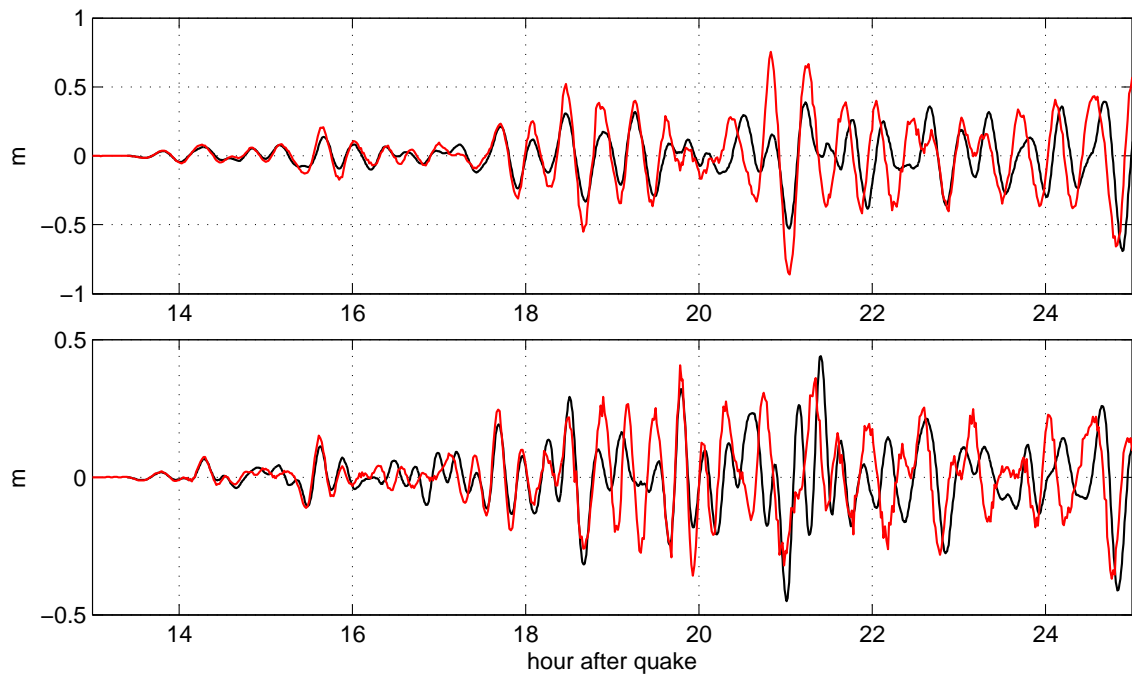


Figure 16: Same as above, for Mega 6 event.

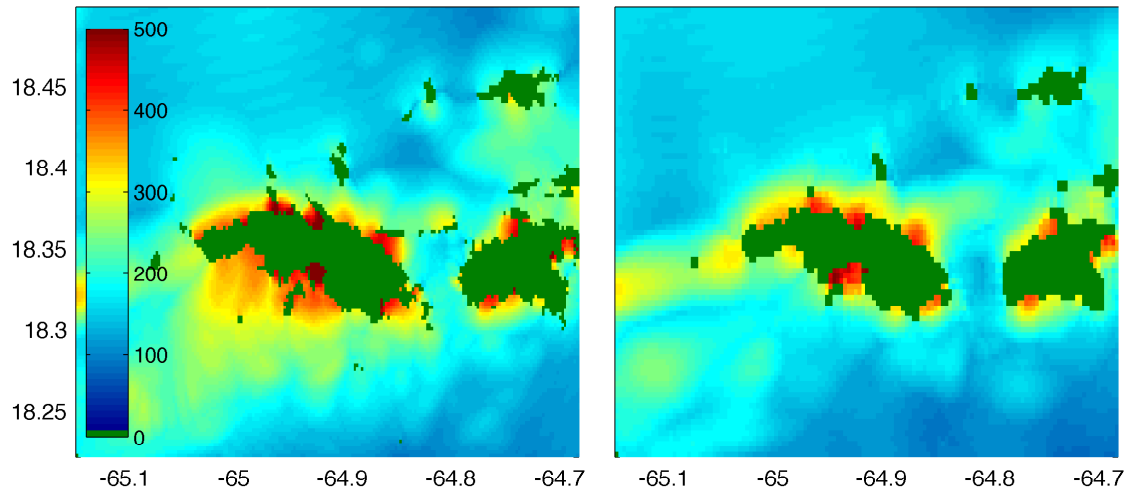


Figure 17: Maximum water elevation with respect to still sea level within B grid, according to Forecast Model (right) and Reference model (left) for Mega 1 event. X-axis: longitude, degree East, Y-axis - latitude, degree North. Colorscale: cm.

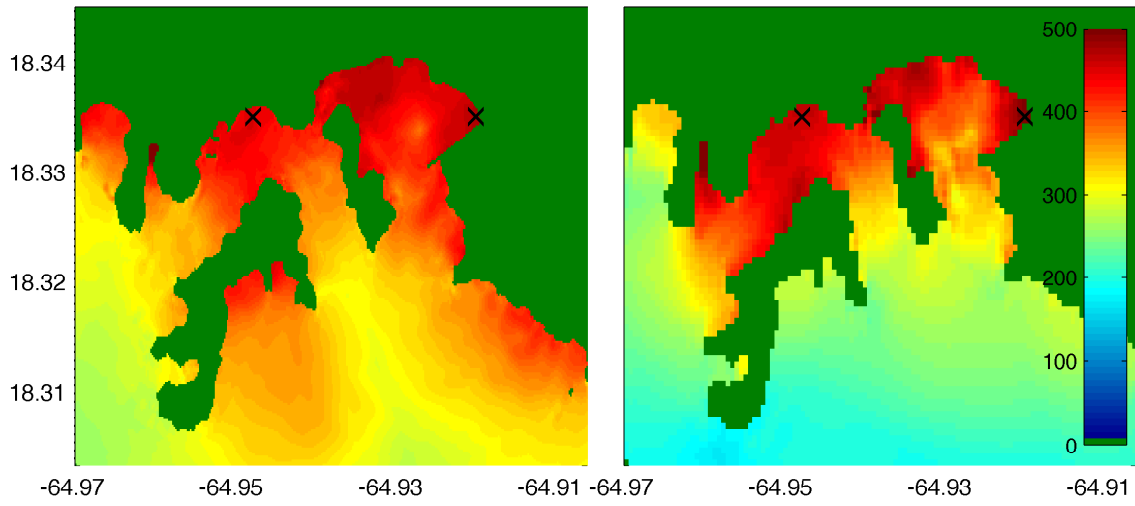


Figure 18: Maximum water elevation with respect to still sea level within C grid, according to Forecast Model (right) and Reference model (left) for Mega 1 event. X-axis: longitude, degree East, Y-axis - latitude, degree North. Colorscale: cm. Crosses: observation points.

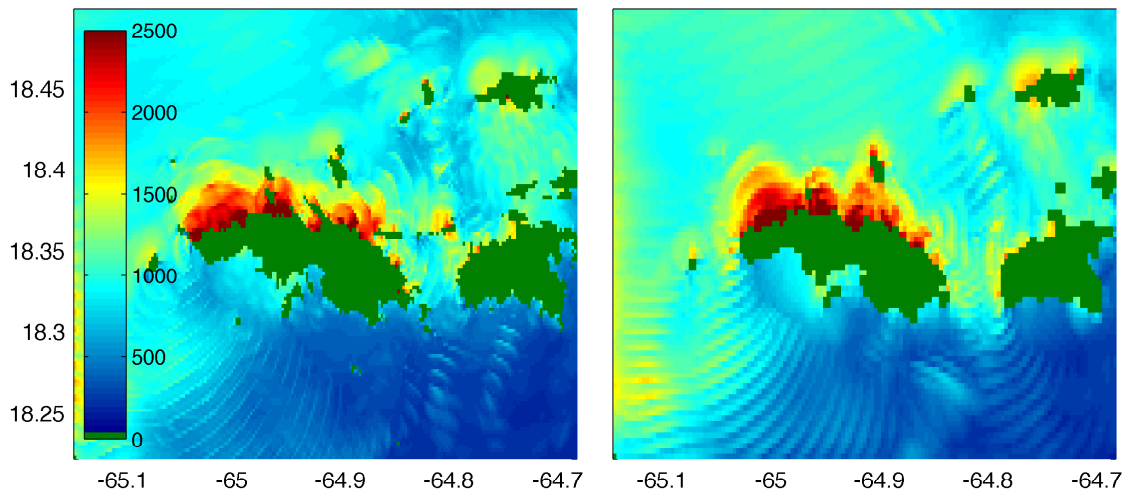


Figure 19: Same as above for Mega 2 event in B grid.

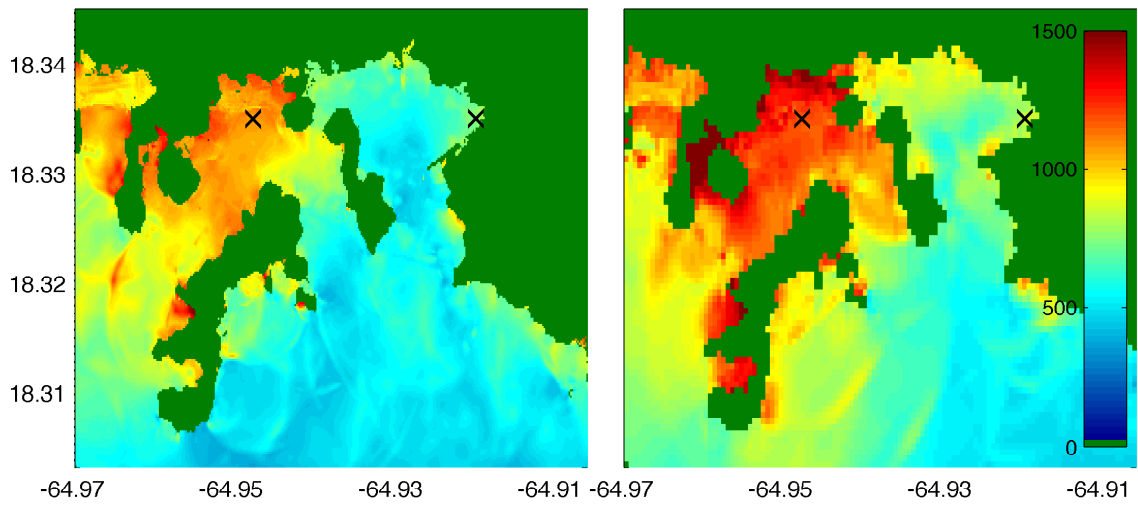


Figure 20: Same as above for Mega 2 event in C grid.

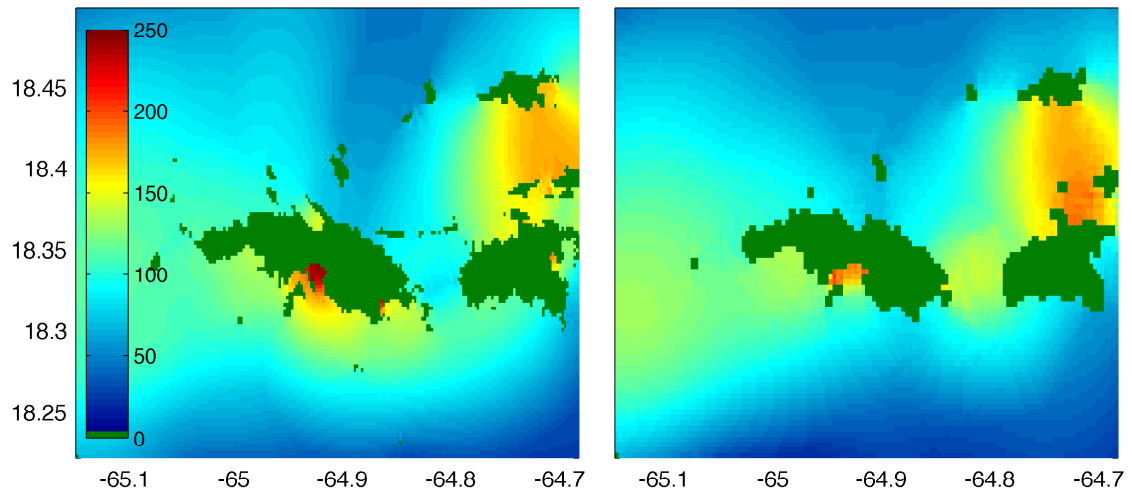


Figure 21: Same as above for Mega 3 event in B grid.

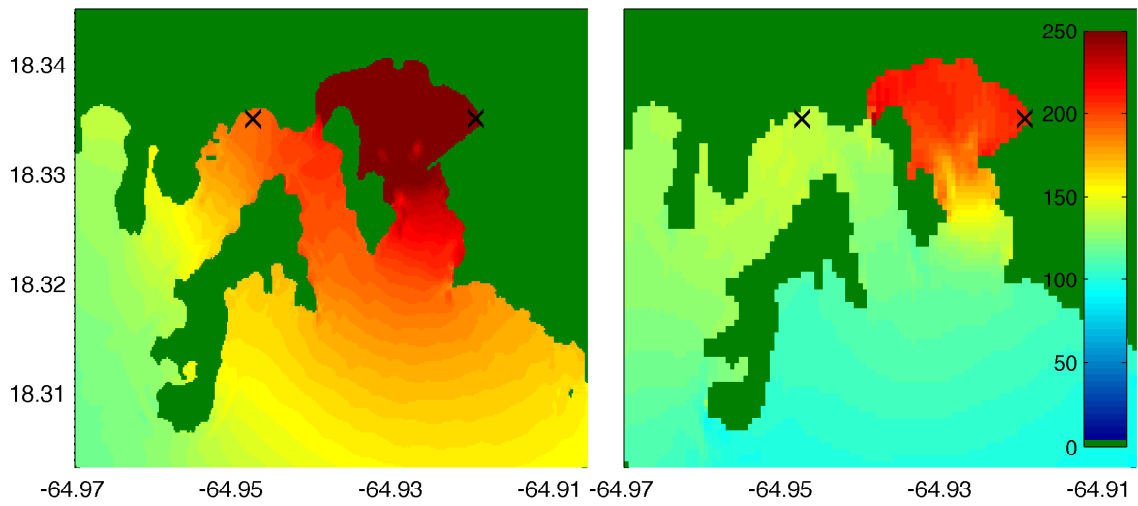


Figure 22: Same as above for Mega 3 event in C grid.

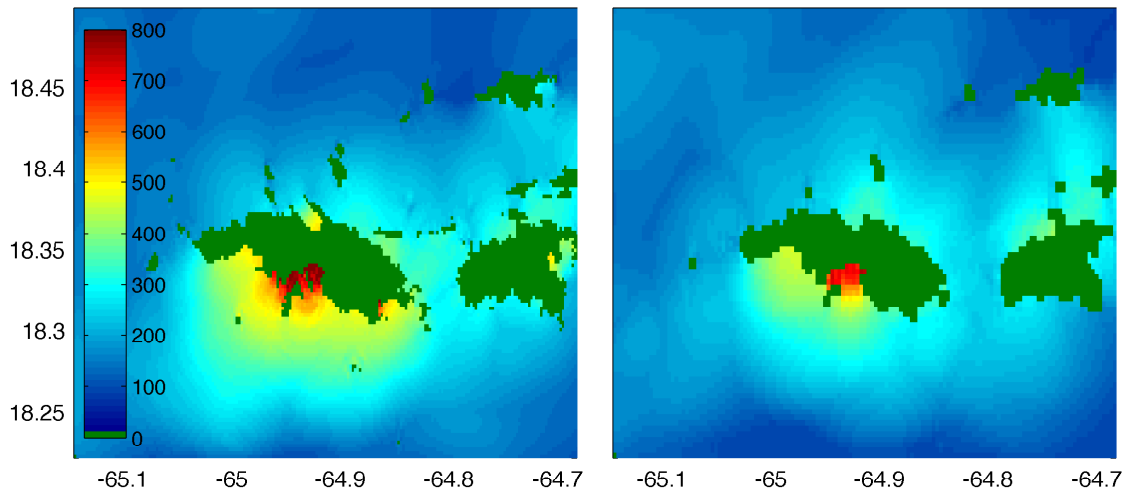


Figure 23: Same as above for Mega 5 event in B grid.

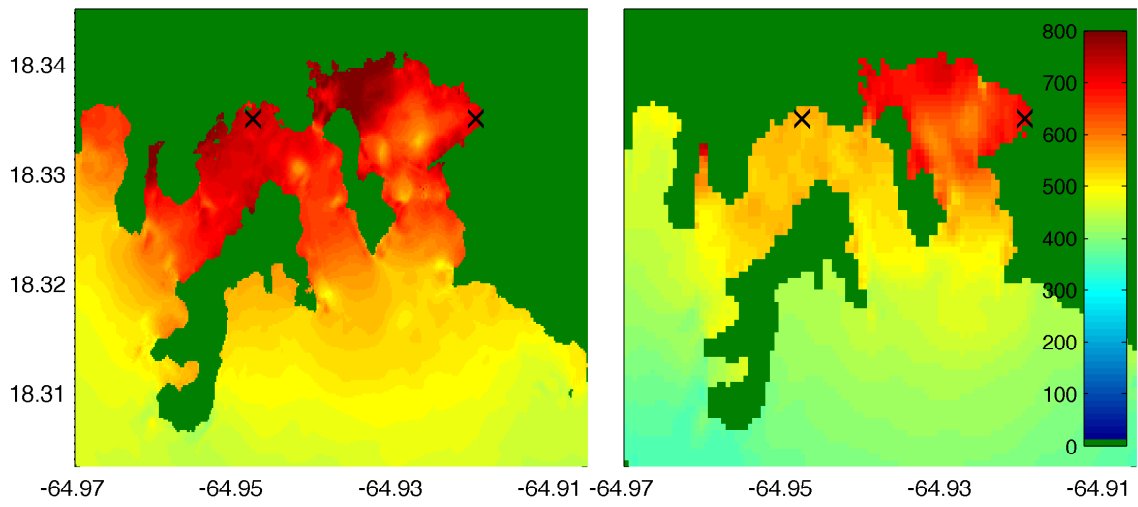


Figure 24: Same as above for Mega 5 event in C grid.

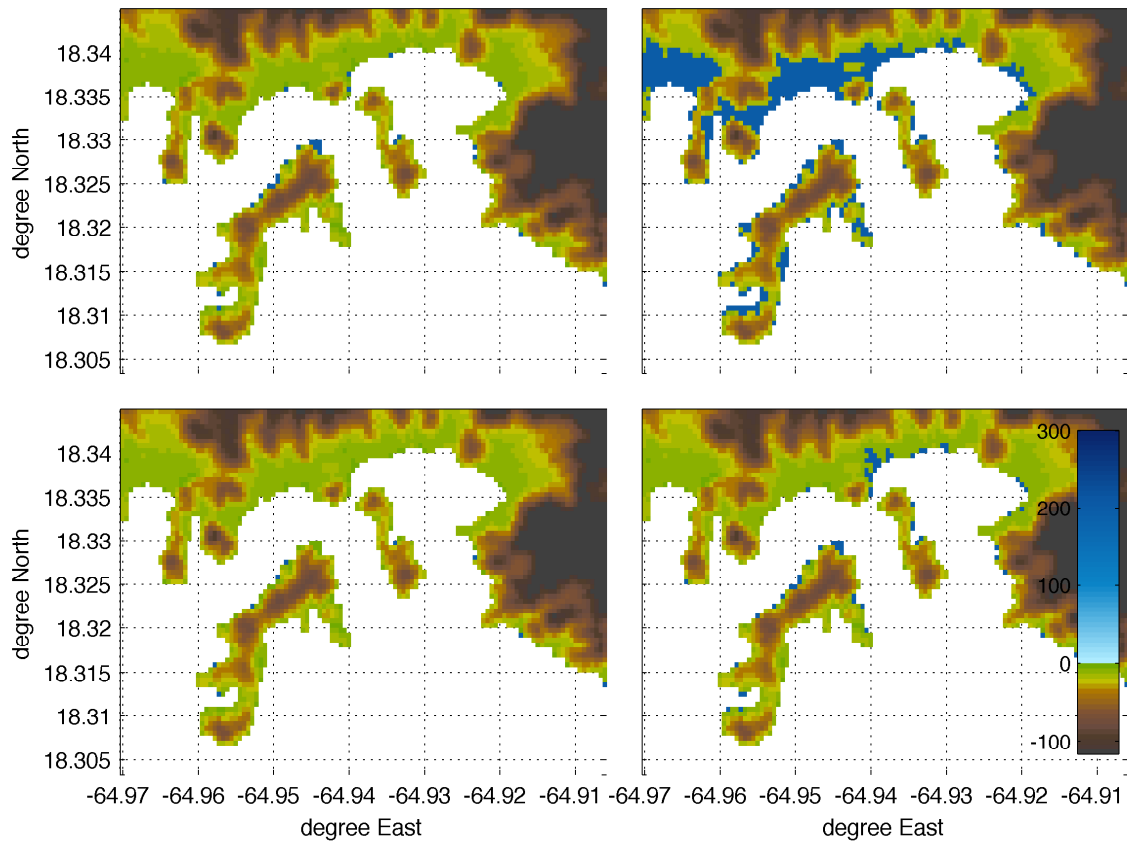


Figure 25: Area inundated by mega tsunamis (event Mega 1 (top left), Mega 2 (top right), Mega 3 (bottom left), and Mega 5 (bottom right)), according to Forecast Model. Only originally dry land is shown, with inundated area shown in blue. Colorscale - meters (does not apply to the inundated area).

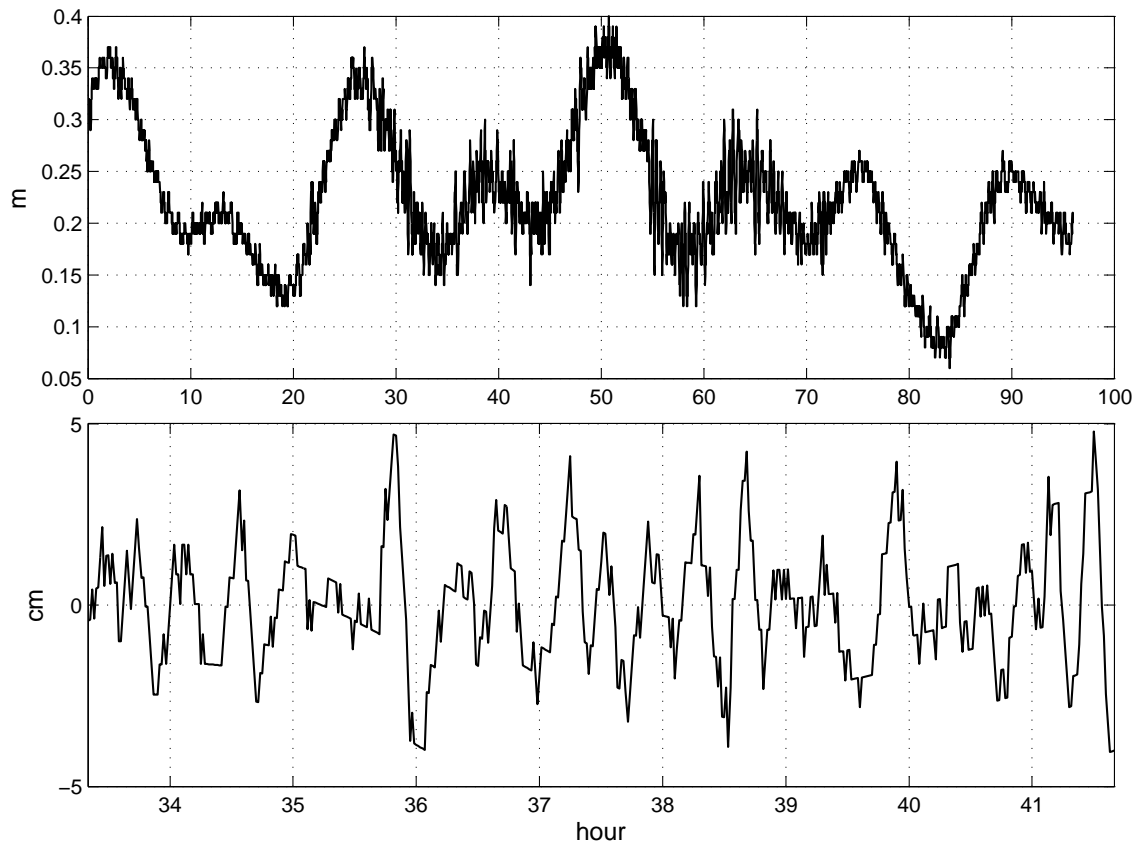


Figure 26: Saint Thomas Harbor gauge sample record (top), segment of the de-tided record (bottom). Time since 00:00 Aug. 1, 2011.

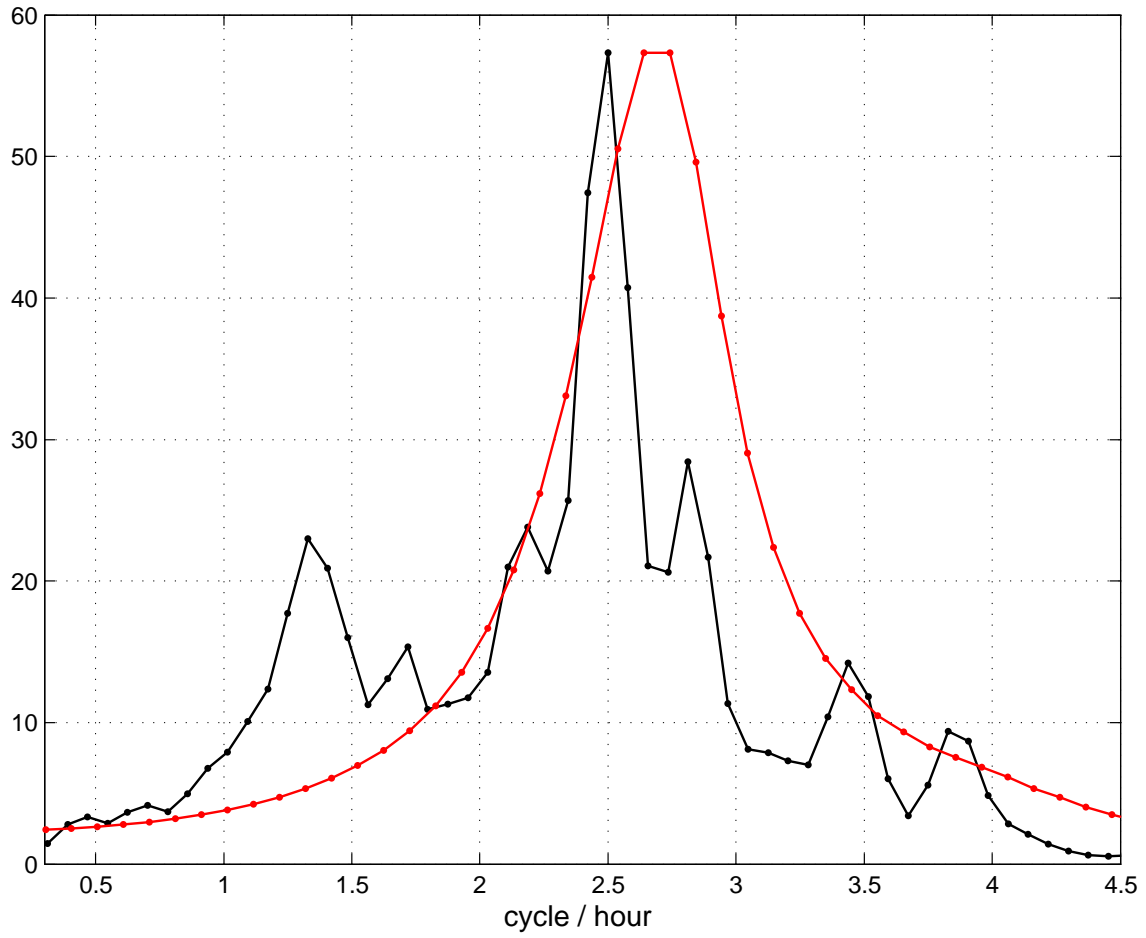


Figure 27: Power spectrum of Saint Thomas Harbor gauge background signal (black) and five-event-averaged power spectrum of the first EOF mode time history (red).

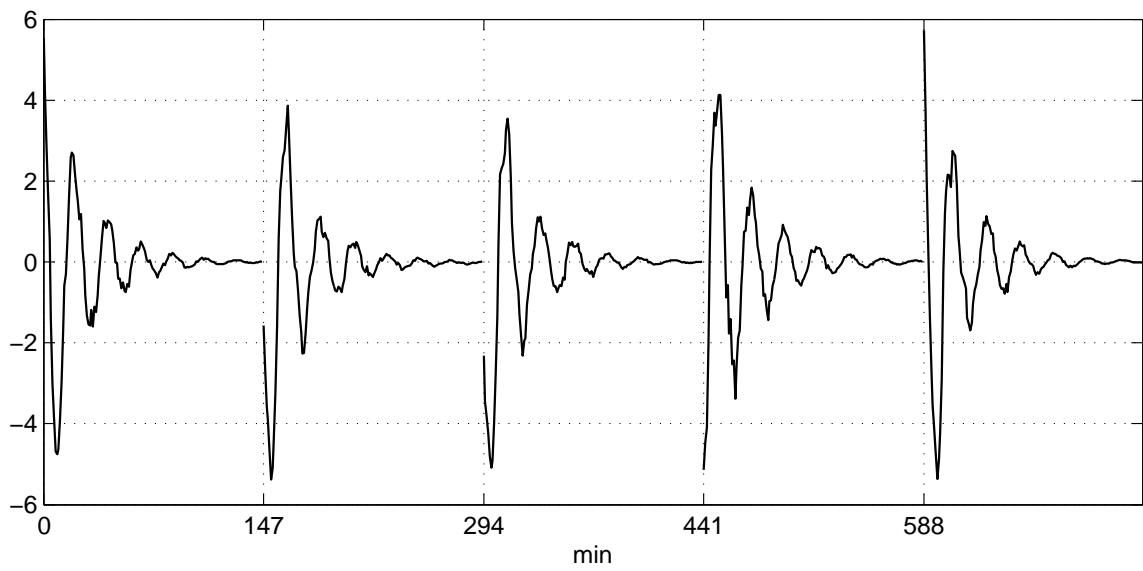


Figure 28: Concatenated fragments of the five simulated tsunamis in a sample node in the harbor, since 310 min from the start of each simulation in grid C. The boundary input into the grid was terminated at 300 min. Each event data set was normalized by its RMS value.

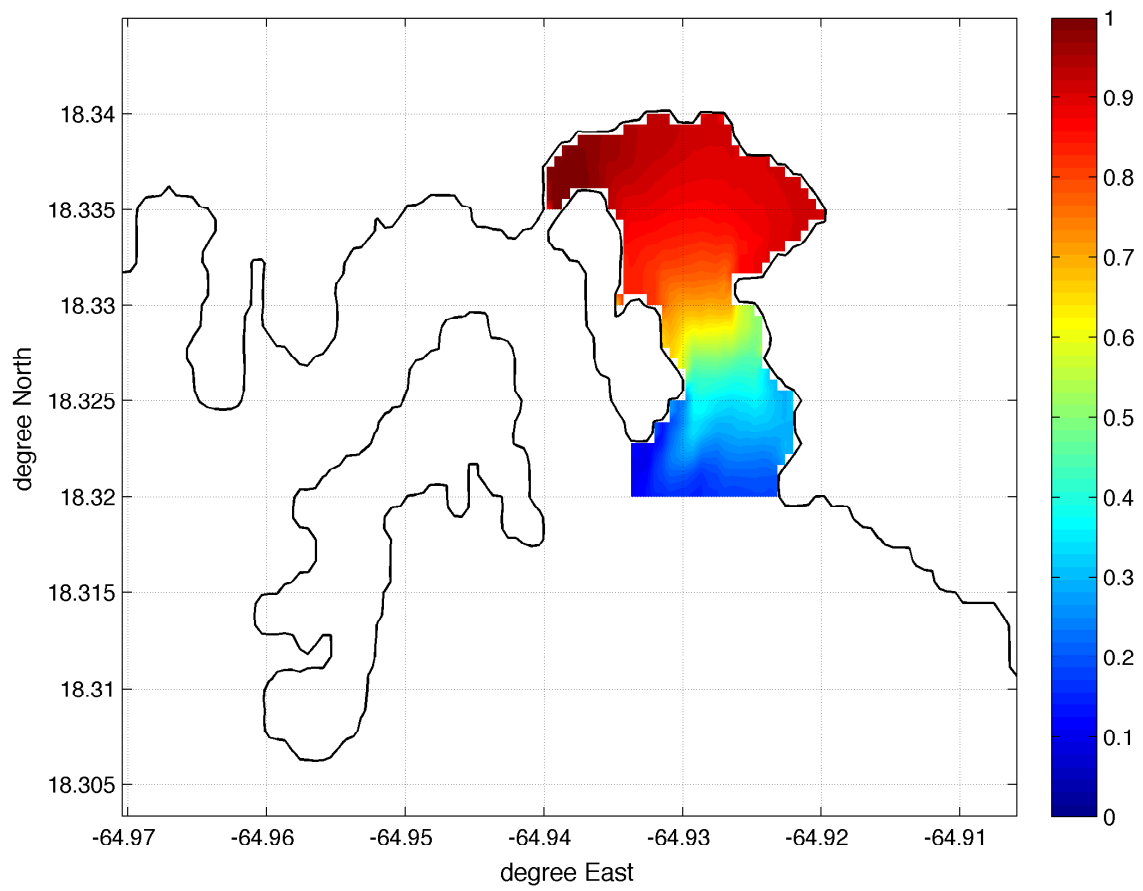


Figure 29: Distribution of the normal oscillation amplitude, as deduced from the amplitude of the first complex EOF mode of concatenated tsunami scenarios.

B Propagation Database: Atlantic Ocean Unit Sources

Propagation source details reflect the database as of January 2010. There may have been updates in the earthquake source parameters after this date.

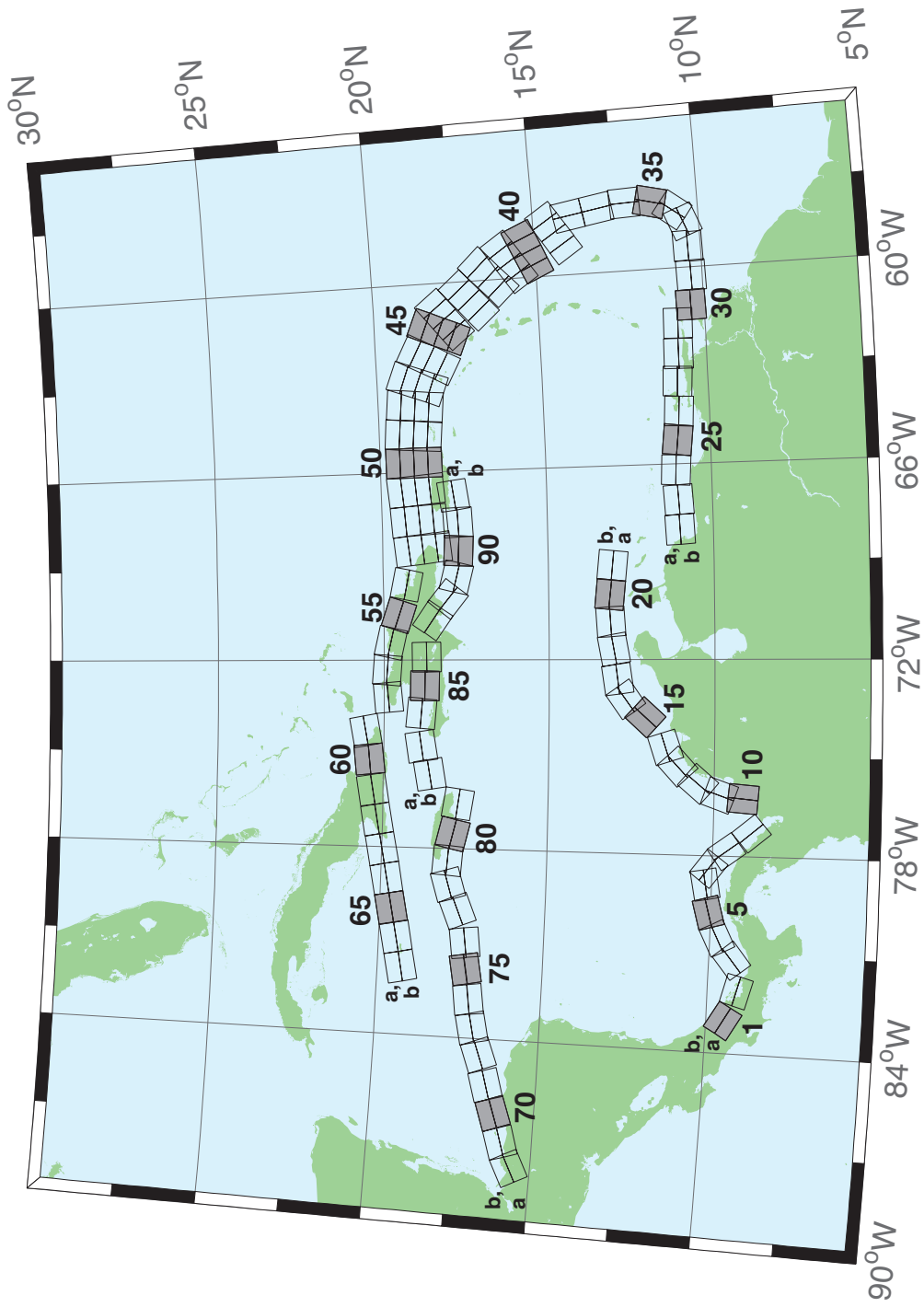


Figure 30: Atlantic Source Zone unit sources.

Table 7: Earthquake parameters for Atlantic Source Zone unit sources.

Segment	Description	Longitude(°E)	Latitude(°N)	Strike(°)	Dip(°)	Depth (km)
atsz-1a	Atlantic Source Zone	-83.2020	9.1449	120	27.5	28.09
atsz-1b	Atlantic Source Zone	-83.0000	9.4899	120	27.5	5
atsz-2a	Atlantic Source Zone	-82.1932	8.7408	105.1	27.5	28.09
atsz-2b	Atlantic Source Zone	-82.0880	9.1254	105.1	27.5	5
atsz-3a	Atlantic Source Zone	-80.9172	9.0103	51.31	30	30
atsz-3b	Atlantic Source Zone	-81.1636	9.3139	51.31	30	5
atsz-4a	Atlantic Source Zone	-80.3265	9.4308	63.49	30	30
atsz-4b	Atlantic Source Zone	-80.5027	9.7789	63.49	30	5
atsz-5a	Atlantic Source Zone	-79.6247	9.6961	74.44	30	30
atsz-5b	Atlantic Source Zone	-79.7307	10.0708	74.44	30	5
atsz-6a	Atlantic Source Zone	-78.8069	9.8083	79.71	30	30
atsz-6b	Atlantic Source Zone	-78.8775	10.1910	79.71	30	5
atsz-7a	Atlantic Source Zone	-78.6237	9.7963	127.2	30	30
atsz-7b	Atlantic Source Zone	-78.3845	10.1059	127.2	30	5
atsz-8a	Atlantic Source Zone	-78.1693	9.3544	143.8	30	30
atsz-8b	Atlantic Source Zone	-77.8511	9.5844	143.8	30	5
atsz-9a	Atlantic Source Zone	-77.5913	8.5989	139.9	30	30
atsz-9b	Atlantic Source Zone	-77.2900	8.8493	139.9	30	5
atsz-10a	Atlantic Source Zone	-75.8109	9.0881	4.67	17	19.62
atsz-10b	Atlantic Source Zone	-76.2445	9.1231	4.67	17	5
atsz-11a	Atlantic Source Zone	-75.7406	9.6929	19.67	17	19.62
atsz-11b	Atlantic Source Zone	-76.1511	9.8375	19.67	17	5
atsz-12a	Atlantic Source Zone	-75.4763	10.2042	40.4	17	19.62
atsz-12b	Atlantic Source Zone	-75.8089	10.4826	40.4	17	5
atsz-13a	Atlantic Source Zone	-74.9914	10.7914	47.17	17	19.62
atsz-13b	Atlantic Source Zone	-75.2890	11.1064	47.17	17	5
atsz-14a	Atlantic Source Zone	-74.5666	11.0708	71.68	17	19.62
atsz-14b	Atlantic Source Zone	-74.7043	11.4786	71.68	17	5
atsz-15a	Atlantic Source Zone	-73.4576	11.8012	42.69	17	19.62
atsz-15b	Atlantic Source Zone	-73.7805	12.0924	42.69	17	5
atsz-16a	Atlantic Source Zone	-72.9788	12.3365	54.75	17	19.62
atsz-16b	Atlantic Source Zone	-73.2329	12.6873	54.75	17	5
atsz-17a	Atlantic Source Zone	-72.5454	12.5061	81.96	17	19.62
atsz-17b	Atlantic Source Zone	-72.6071	12.9314	81.96	17	5
atsz-18a	Atlantic Source Zone	-71.6045	12.6174	79.63	17	19.62
atsz-18b	Atlantic Source Zone	-71.6839	13.0399	79.63	17	5
atsz-19a	Atlantic Source Zone	-70.7970	12.7078	86.32	17	19.62
atsz-19b	Atlantic Source Zone	-70.8253	13.1364	86.32	17	5
atsz-20a	Atlantic Source Zone	-70.0246	12.7185	95.94	17	19.62
atsz-20b	Atlantic Source Zone	-69.9789	13.1457	95.94	17	5
atsz-21a	Atlantic Source Zone	-69.1244	12.6320	95.94	17	19.62
atsz-21b	Atlantic Source Zone	-69.0788	13.0592	95.94	17	5
atsz-22a	Atlantic Source Zone	-68.0338	11.4286	266.9	15	17.94
atsz-22b	Atlantic Source Zone	-68.0102	10.9954	266.9	15	5
atsz-23a	Atlantic Source Zone	-67.1246	11.4487	266.9	15	17.94
atsz-23b	Atlantic Source Zone	-67.1010	11.0155	266.9	15	5
atsz-24a	Atlantic Source Zone	-66.1656	11.5055	273.3	15	17.94
atsz-24b	Atlantic Source Zone	-66.1911	11.0724	273.3	15	5
atsz-25a	Atlantic Source Zone	-65.2126	11.4246	276.4	15	17.94
atsz-25b	Atlantic Source Zone	-65.2616	10.9934	276.4	15	5
atsz-26a	Atlantic Source Zone	-64.3641	11.3516	272.9	15	17.94
atsz-26b	Atlantic Source Zone	-64.3862	10.9183	272.9	15	5
atsz-27a	Atlantic Source Zone	-63.4472	11.3516	272.9	15	17.94
atsz-27b	Atlantic Source Zone	-63.4698	10.9183	272.9	15	5
atsz-28a	Atlantic Source Zone	-62.6104	11.2831	271.1	15	17.94
atsz-28b	Atlantic Source Zone	-62.6189	10.8493	271.1	15	5
atsz-29a	Atlantic Source Zone	-61.6826	11.2518	271.6	15	17.94
atsz-29b	Atlantic Source Zone	-61.6947	10.8181	271.6	15	5
atsz-30a	Atlantic Source Zone	-61.1569	10.8303	269	15	17.94
atsz-30b	Atlantic Source Zone	-61.1493	10.3965	269	15	5
atsz-31a	Atlantic Source Zone	-60.2529	10.7739	269	15	17.94
atsz-31b	Atlantic Source Zone	-60.2453	10.3401	269	15	5
atsz-32a	Atlantic Source Zone	-59.3510	10.8123	269	15	17.94
atsz-32b	Atlantic Source Zone	-59.3734	10.3785	269	15	5
atsz-33a	Atlantic Source Zone	-58.7592	10.8785	248.6	15	17.94

Continued on next page

Table 7 – continued from previous page

Segment	Description	Longitude(°E)	Latitude(°N)	Strike(°)	Dip(°)	Depth (km)
atsz-33b	Atlantic Source Zone	-58.5984	10.4745	248.6	15	5
atsz-34a	Atlantic Source Zone	-58.5699	11.0330	217.2	15	17.94
atsz-34b	Atlantic Source Zone	-58.2179	10.7710	217.2	15	5
atsz-35a	Atlantic Source Zone	-58.3549	11.5300	193.7	15	17.94
atsz-35b	Atlantic Source Zone	-57.9248	11.4274	193.7	15	5
atsz-36a	Atlantic Source Zone	-58.3432	12.1858	177.7	15	17.94
atsz-36b	Atlantic Source Zone	-57.8997	12.2036	177.7	15	5
atsz-37a	Atlantic Source Zone	-58.4490	12.9725	170.7	15	17.94
atsz-37b	Atlantic Source Zone	-58.0095	13.0424	170.7	15	5
atsz-38a	Atlantic Source Zone	-58.6079	13.8503	170.2	15	17.94
atsz-38b	Atlantic Source Zone	-58.1674	13.9240	170.2	15	5
atsz-39a	Atlantic Source Zone	-58.6667	14.3915	146.8	15	17.94
atsz-39b	Atlantic Source Zone	-58.2913	14.6287	146.8	15	5
atsz-39y	Atlantic Source Zone	-59.4168	13.9171	146.8	15	43.82
atsz-39z	Atlantic Source Zone	-59.0415	14.1543	146.8	15	30.88
atsz-40a	Atlantic Source Zone	-59.1899	15.2143	156.2	15	17.94
atsz-40b	Atlantic Source Zone	-58.7781	15.3892	156.2	15	5
atsz-40y	Atlantic Source Zone	-60.0131	14.8646	156.2	15	43.82
atsz-40z	Atlantic Source Zone	-59.6012	15.0395	156.2	15	30.88
atsz-41a	Atlantic Source Zone	-59.4723	15.7987	146.3	15	17.94
atsz-41b	Atlantic Source Zone	-59.0966	16.0392	146.3	15	5
atsz-41y	Atlantic Source Zone	-60.2229	15.3177	146.3	15	43.82
atsz-41z	Atlantic Source Zone	-59.8473	15.5582	146.3	15	30.88
atsz-42a	Atlantic Source Zone	-59.9029	16.4535	137	15	17.94
atsz-42b	Atlantic Source Zone	-59.5716	16.7494	137	15	5
atsz-42y	Atlantic Source Zone	-60.5645	15.8616	137	15	43.82
atsz-42z	Atlantic Source Zone	-60.2334	16.1575	137	15	30.88
atsz-43a	Atlantic Source Zone	-60.5996	17.0903	138.7	15	17.94
atsz-43b	Atlantic Source Zone	-60.2580	17.3766	138.7	15	5
atsz-43y	Atlantic Source Zone	-61.2818	16.5177	138.7	15	43.82
atsz-43z	Atlantic Source Zone	-60.9404	16.8040	138.7	15	30.88
atsz-44a	Atlantic Source Zone	-61.1559	17.8560	141.1	15	17.94
atsz-44b	Atlantic Source Zone	-60.8008	18.1286	141.1	15	5
atsz-44y	Atlantic Source Zone	-61.8651	17.3108	141.1	15	43.82
atsz-44z	Atlantic Source Zone	-61.5102	17.5834	141.1	15	30.88
atsz-45a	Atlantic Source Zone	-61.5491	18.0566	112.8	15	17.94
atsz-45b	Atlantic Source Zone	-61.3716	18.4564	112.8	15	5
atsz-45y	Atlantic Source Zone	-61.9037	17.2569	112.8	15	43.82
atsz-45z	Atlantic Source Zone	-61.7260	17.6567	112.8	15	30.88
atsz-46a	Atlantic Source Zone	-62.4217	18.4149	117.9	15	17.94
atsz-46b	Atlantic Source Zone	-62.2075	18.7985	117.9	15	5
atsz-46y	Atlantic Source Zone	-62.8493	17.6477	117.9	15	43.82
atsz-46z	Atlantic Source Zone	-62.6352	18.0313	117.9	15	30.88
atsz-47a	Atlantic Source Zone	-63.1649	18.7844	110.5	20	22.1
atsz-47b	Atlantic Source Zone	-63.0087	19.1798	110.5	20	5
atsz-47y	Atlantic Source Zone	-63.4770	17.9936	110.5	20	56.3
atsz-47z	Atlantic Source Zone	-63.3205	18.3890	110.5	20	39.2
atsz-48a	Atlantic Source Zone	-63.8800	18.8870	95.37	20	22.1
atsz-48b	Atlantic Source Zone	-63.8382	19.3072	95.37	20	5
atsz-48y	Atlantic Source Zone	-63.9643	18.0465	95.37	20	56.3
atsz-48z	Atlantic Source Zone	-63.9216	18.4667	95.37	20	39.2
atsz-49a	Atlantic Source Zone	-64.8153	18.9650	94.34	20	22.1
atsz-49b	Atlantic Source Zone	-64.7814	19.3859	94.34	20	5
atsz-49y	Atlantic Source Zone	-64.8840	18.1233	94.34	20	56.3
atsz-49z	Atlantic Source Zone	-64.8492	18.5442	94.34	20	39.2
atsz-50a	Atlantic Source Zone	-65.6921	18.9848	89.59	20	22.1
atsz-50b	Atlantic Source Zone	-65.6953	19.4069	89.59	20	5
atsz-50y	Atlantic Source Zone	-65.6874	18.1407	89.59	20	56.3
atsz-50z	Atlantic Source Zone	-65.6887	18.5628	89.59	20	39.2
atsz-51a	Atlantic Source Zone	-66.5742	18.9484	84.98	20	22.1
atsz-51b	Atlantic Source Zone	-66.6133	19.3688	84.98	20	5
atsz-51y	Atlantic Source Zone	-66.4977	18.1076	84.98	20	56.3
atsz-51z	Atlantic Source Zone	-66.5353	18.5280	84.98	20	39.2
atsz-52a	Atlantic Source Zone	-67.5412	18.8738	85.87	20	22.1
atsz-52b	Atlantic Source Zone	-67.5734	19.2948	85.87	20	5
atsz-52y	Atlantic Source Zone	-67.4781	18.0319	85.87	20	56.3

Continued on next page

Table 7 – continued from previous page

Segment	Description	Longitude(°E)	Latitude(°N)	Strike(°)	Dip(°)	Depth (km)
atsz-52z	Atlantic Source Zone	-67.5090	18.4529	85.87	20	39.2
atsz-53a	Atlantic Source Zone	-68.4547	18.7853	83.64	20	22.1
atsz-53b	Atlantic Source Zone	-68.5042	19.2048	83.64	20	5
atsz-53y	Atlantic Source Zone	-68.3575	17.9463	83.64	20	56.3
atsz-53z	Atlantic Source Zone	-68.4055	18.3658	83.64	20	39.2
atsz-54a	Atlantic Source Zone	-69.6740	18.8841	101.5	20	22.1
atsz-54b	Atlantic Source Zone	-69.5846	19.2976	101.5	20	5
atsz-55a	Atlantic Source Zone	-70.7045	19.1376	108.2	20	22.1
atsz-55b	Atlantic Source Zone	-70.5647	19.5386	108.2	20	5
atsz-56a	Atlantic Source Zone	-71.5368	19.3853	102.6	20	22.1
atsz-56b	Atlantic Source Zone	-71.4386	19.7971	102.6	20	5
atsz-57a	Atlantic Source Zone	-72.3535	19.4838	94.2	20	22.1
atsz-57b	Atlantic Source Zone	-72.3206	19.9047	94.2	20	5
atsz-58a	Atlantic Source Zone	-73.1580	19.4498	84.34	20	22.1
atsz-58b	Atlantic Source Zone	-73.2022	19.8698	84.34	20	5
atsz-59a	Atlantic Source Zone	-74.3567	20.9620	259.7	20	22.1
atsz-59b	Atlantic Source Zone	-74.2764	20.5467	259.7	20	5
atsz-60a	Atlantic Source Zone	-75.2386	20.8622	264.2	15	17.94
atsz-60b	Atlantic Source Zone	-75.1917	20.4306	264.2	15	5
atsz-61a	Atlantic Source Zone	-76.2383	20.7425	260.7	15	17.94
atsz-61b	Atlantic Source Zone	-76.1635	20.3144	260.7	15	5
atsz-62a	Atlantic Source Zone	-77.2021	20.5910	259.9	15	17.94
atsz-62b	Atlantic Source Zone	-77.1214	20.1638	259.9	15	5
atsz-63a	Atlantic Source Zone	-78.1540	20.4189	259	15	17.94
atsz-63b	Atlantic Source Zone	-78.0661	19.9930	259	15	5
atsz-64a	Atlantic Source Zone	-79.0959	20.2498	259.2	15	17.94
atsz-64b	Atlantic Source Zone	-79.0098	19.8236	259.2	15	5
atsz-65a	Atlantic Source Zone	-80.0393	20.0773	258.9	15	17.94
atsz-65b	Atlantic Source Zone	-79.9502	19.6516	258.9	15	5
atsz-66a	Atlantic Source Zone	-80.9675	19.8993	258.6	15	17.94
atsz-66b	Atlantic Source Zone	-80.8766	19.4740	258.6	15	5
atsz-67a	Atlantic Source Zone	-81.9065	19.7214	258.5	15	17.94
atsz-67b	Atlantic Source Zone	-81.8149	19.2962	258.5	15	5
atsz-68a	Atlantic Source Zone	-87.8003	15.2509	62.69	15	17.94
atsz-68b	Atlantic Source Zone	-88.0070	15.6364	62.69	15	5
atsz-69a	Atlantic Source Zone	-87.0824	15.5331	72.73	15	17.94
atsz-69b	Atlantic Source Zone	-87.2163	15.9474	72.73	15	5
atsz-70a	Atlantic Source Zone	-86.1622	15.8274	70.64	15	17.94
atsz-70b	Atlantic Source Zone	-86.3120	16.2367	70.64	15	5
atsz-71a	Atlantic Source Zone	-85.3117	16.1052	73.7	15	17.94
atsz-71b	Atlantic Source Zone	-85.4387	16.5216	73.7	15	5
atsz-72a	Atlantic Source Zone	-84.3470	16.3820	69.66	15	17.94
atsz-72b	Atlantic Source Zone	-84.5045	16.7888	69.66	15	5
atsz-73a	Atlantic Source Zone	-83.5657	16.6196	77.36	15	17.94
atsz-73b	Atlantic Source Zone	-83.6650	17.0429	77.36	15	5
atsz-74a	Atlantic Source Zone	-82.7104	16.7695	82.35	15	17.94
atsz-74b	Atlantic Source Zone	-82.7709	17.1995	82.35	15	5
atsz-75a	Atlantic Source Zone	-81.7297	16.9003	79.86	15	17.94
atsz-75b	Atlantic Source Zone	-81.8097	17.3274	79.86	15	5
atsz-76a	Atlantic Source Zone	-80.9196	16.9495	82.95	15	17.94
atsz-76b	Atlantic Source Zone	-80.9754	17.3801	82.95	15	5
atsz-77a	Atlantic Source Zone	-79.8086	17.2357	67.95	15	17.94
atsz-77b	Atlantic Source Zone	-79.9795	17.6378	67.95	15	5
atsz-78a	Atlantic Source Zone	-79.0245	17.5415	73.61	15	17.94
atsz-78b	Atlantic Source Zone	-79.1532	17.9577	73.61	15	5
atsz-79a	Atlantic Source Zone	-78.4122	17.5689	94.07	15	17.94
atsz-79b	Atlantic Source Zone	-78.3798	18.0017	94.07	15	5
atsz-80a	Atlantic Source Zone	-77.6403	17.4391	103.3	15	17.94
atsz-80b	Atlantic Source Zone	-77.5352	17.8613	103.3	15	5
atsz-81a	Atlantic Source Zone	-76.6376	17.2984	98.21	15	17.94
atsz-81b	Atlantic Source Zone	-76.5726	17.7278	98.21	15	5
atsz-82a	Atlantic Source Zone	-75.7299	19.0217	260.1	15	17.94
atsz-82b	Atlantic Source Zone	-75.6516	18.5942	260.1	15	5
atsz-83a	Atlantic Source Zone	-74.8351	19.2911	260.8	15	17.94
atsz-83b	Atlantic Source Zone	-74.7621	18.8628	260.8	15	5
atsz-84a	Atlantic Source Zone	-73.6639	19.2991	274.8	15	17.94

Continued on next page

Table 7 – continued from previous page

Segment	Description	Longitude(°E)	Latitude(°N)	Strike(°)	Dip(°)	Depth (km)
atsz-84b	Atlantic Source Zone	-73.7026	18.8668	274.8	15	5
atsz-85a	Atlantic Source Zone	-72.8198	19.2019	270.6	15	17.94
atsz-85b	Atlantic Source Zone	-72.8246	18.7681	270.6	15	5
atsz-86a	Atlantic Source Zone	-71.9143	19.1477	269.1	15	17.94
atsz-86b	Atlantic Source Zone	-71.9068	18.7139	269.1	15	5
atsz-87a	Atlantic Source Zone	-70.4738	18.8821	304.5	15	17.94
atsz-87b	Atlantic Source Zone	-70.7329	18.5245	304.5	15	5
atsz-88a	Atlantic Source Zone	-69.7710	18.3902	308.9	15	17.94
atsz-88b	Atlantic Source Zone	-70.0547	18.0504	308.4	15	5
atsz-89a	Atlantic Source Zone	-69.2635	18.2099	283.9	15	17.94
atsz-89b	Atlantic Source Zone	-69.3728	17.7887	283.9	15	5
atsz-90a	Atlantic Source Zone	-68.5059	18.1443	272.9	15	17.94
atsz-90b	Atlantic Source Zone	-68.5284	17.7110	272.9	15	5
atsz-91a	Atlantic Source Zone	-67.6428	18.1438	267.8	15	17.94
atsz-91b	Atlantic Source Zone	-67.6256	17.7103	267.8	15	5
atsz-92a	Atlantic Source Zone	-66.8261	18.2536	262	15	17.94
atsz-92b	Atlantic Source Zone	-66.7627	17.8240	262	15	5

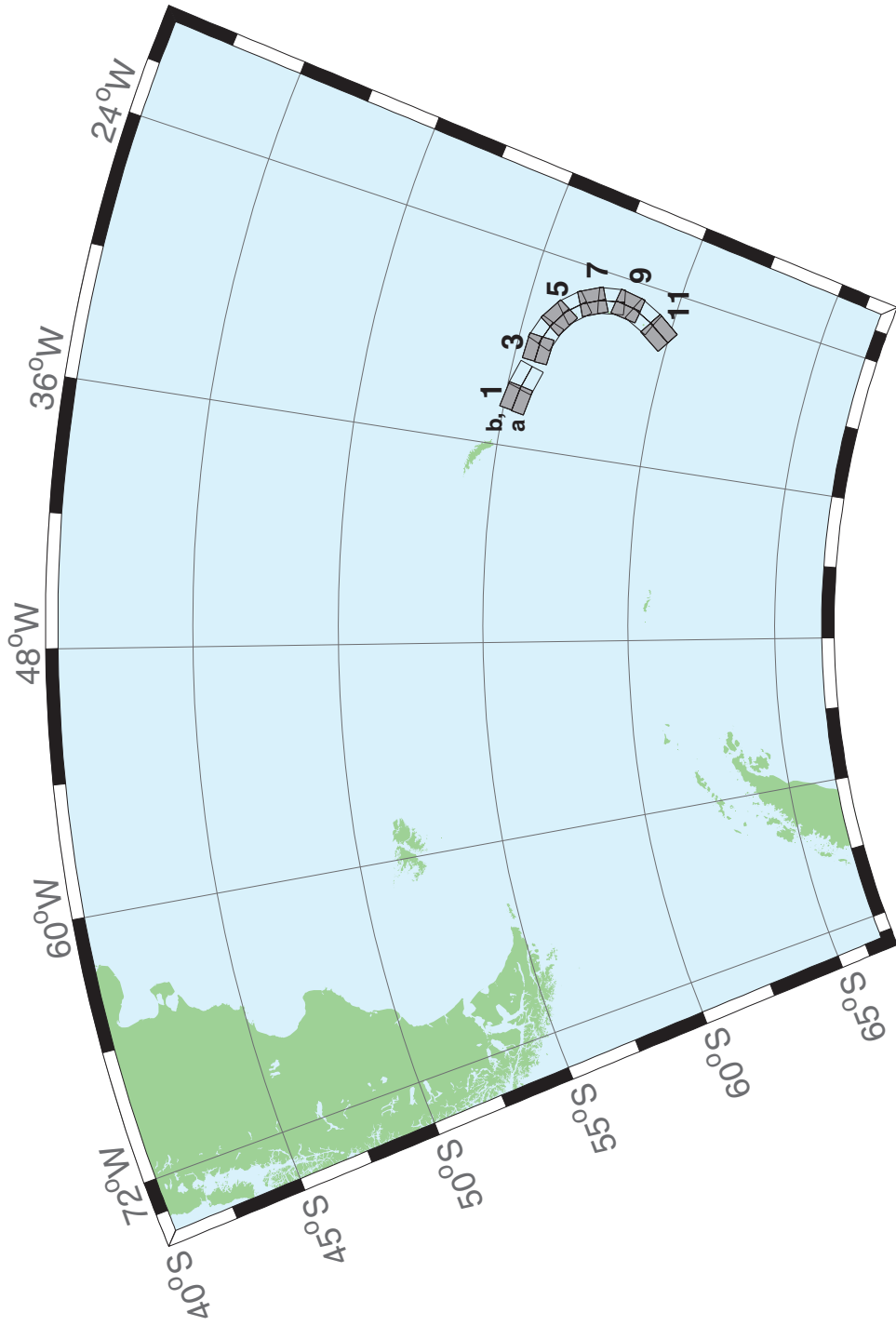


Figure 31: South Sandwich Islands Subduction Zone.

Table 8: Earthquake parameters for South Sandwich Islands Subduction Zone unit sources.

Segment	Description	Longitude(°E)	Latitude(°N)	Strike(°)	Dip(°)	Depth (km)
sssz-1a	South Sandwich Islands Subduction Zone	-33.0670	-55.3780	280.2	15	17.94
sssz-1b	South Sandwich Islands Subduction Zone	-32.9242	-54.9510	280.2	15	5
sssz-2a	South Sandwich Islands Subduction Zone	-31.7197	-55.5621	286.3	15	17.94
sssz-2b	South Sandwich Islands Subduction Zone	-31.4969	-55.1457	286.3	15	5
sssz-3a	South Sandwich Islands Subduction Zone	-29.8355	-55.7456	273	15	17.94
sssz-3b	South Sandwich Islands Subduction Zone	-29.7873	-55.3123	273	15	5
sssz-4a	South Sandwich Islands Subduction Zone	-28.7648	-55.8715	290	15	17.94
sssz-4b	South Sandwich Islands Subduction Zone	-28.4930	-55.4638	290	15	5
sssz-5a	South Sandwich Islands Subduction Zone	-27.6356	-56.1844	301.5	15	17.94
sssz-5b	South Sandwich Islands Subduction Zone	-27.2218	-55.8143	301.5	15	5
sssz-6a	South Sandwich Islands Subduction Zone	-26.7655	-56.5959	317.5	15	17.94
sssz-6b	South Sandwich Islands Subduction Zone	-26.1774	-56.3029	317.5	15	5
sssz-7a	South Sandwich Islands Subduction Zone	-26.0921	-57.1441	332.1	15	17.94
sssz-7b	South Sandwich Islands Subduction Zone	-25.3776	-56.9411	332.1	15	5
sssz-8a	South Sandwich Islands Subduction Zone	-25.7129	-57.7563	347.9	15	17.94
sssz-8b	South Sandwich Islands Subduction Zone	-24.9088	-57.6652	347.9	15	5
sssz-9a	South Sandwich Islands Subduction Zone	-25.7003	-58.3505	7.182	15	17.94
sssz-9b	South Sandwich Islands Subduction Zone	-24.8687	-58.4047	7.182	15	5
sssz-10a	South Sandwich Islands Subduction Zone	-26.0673	-58.9577	24.25	15	17.94
sssz-10b	South Sandwich Islands Subduction Zone	-25.2869	-59.1359	24.25	15	5
sssz-11a	South Sandwich Islands Subduction Zone	-26.8279	-59.6329	32.7	15	17.94
sssz-11b	South Sandwich Islands Subduction Zone	-26.0913	-59.8673	32.7	15	5

C SIFT Testing

By Lindsey Wright and Elena Tolkova

C.1 PURPOSE

Forecast models are tested with synthetic tsunami events covering a range of tsunami source locations and magnitudes. Testing is also done with selected historical tsunami events when available.

The testing of a forecast model has three objectives. The first objective is to assure that the results obtained with the NOAAs tsunami forecast system software, which has been released to the Tsunami Warning Centers for operational use, are consistent with those obtained by the researcher during the development of the forecast model. The second objective is to test the forecast model for consistency, accuracy, time efficiency, and quality of results over a range of possible tsunami locations and magnitudes. The third objective is to identify bugs and issues in need of resolution by the researcher who developed the Forecast Model or by the forecast system software development team before the next version release to NOAAs two Tsunami Warning Centers.

Local hardware and software applications, and tools familiar to the researcher(s), are used to run the Method of Splitting Tsunamis (MOST) model during the forecast model development. The test results presented in this report lend confidence that the model performs as developed and produces the same results when initiated within the forecast system application in an operational setting as those produced by the researcher during the forecast model development. The test results assure those who rely on the Charlotte Amalie tsunami forecast model that consistent results are produced irrespective of system.

C.2 TESTING PROCEDURE

The general procedure for forecast model testing is to run a set of synthetic tsunami scenarios and a selected set of historical tsunami events through the forecast system application and compare the results with those obtained by the researcher during the forecast model development and presented in the Tsunami Forecast Model Report. Specific steps taken to test the model include:

- Identification of testing scenarios, including the standard set of synthetic events, appropriate historical events, and customized synthetic scenarios that may have been used by the researcher(s) in developing the forecast model.
- Creation of new events to represent customized synthetic scenarios used by the researcher(s) in developing the forecast model, if any.
- Submission of test model runs with the forecast system, and export of the results from A, B, and C grids, along with time series.
- Recording applicable metadata, including the specific forecast system version used for testing.
- Examination of forecast model results for instabilities in both time series and plot results.

- Comparison of forecast model results obtained through the forecast system with those obtained during the forecast model development.
- Summarization of results with specific mention of quality, consistency, and time efficiency.
- Reporting of issues identified to modeler and forecast system software development team.
- Retesting the forecast models in the forecast system when reported issues have been addressed or explained.

Synthetic model runs were tested on a DELL PowerEdge R510 computer equipped with two Xeon E5670 processors at 2.93 Ghz, each with 12 MBytes of cache and 32GB memory. The processors are hex core and support hyperthreading, resulting in the computer performing as a 24 processor core machine. Additionally, the testing computer supports 10 Gigabit Ethernet for fast network connections. This computer configuration is similar or the same as the configurations of the computers installed at the Tsunami Warning Centers so the compute times should only vary slightly.

C.3 Results

The Charlotte Amalie forecast model was tested with SIFT version 3.2.

The Charlotte Amalie, Virgin Islands forecast model was tested with three synthetic scenarios. Test results from the forecast system and comparisons with the results obtained during the forecast model development are shown numerically in Table 1 and graphically in Figures 32 to 34. The results show that the minimum and maximum amplitudes and time series obtained from the forecast system agree with those obtained during the forecast model development, and that the forecast model is stable and robust, with consistent and high quality results across geographically distributed tsunami sources. The model run time (wall clock time) was 7.30 minutes for 9.99 hours of simulation time, and 2.92 minutes for 4.0 hours. This run time is well within the 10 minute run time for 4 hours of simulation time.

A suite of three synthetic events was run on the Charlotte Amalie forecast model. The modeled scenarios were stable for all cases run. Wave heights greater than 500 centimeters (cm) were observed from the Atlantic (ATSZ 38-47, ATSZ 48-57) source zone. The largest modeled height was 769 cm from the Atlantic (ATSZ 48-57) source zone. The smallest signal of 66 cm was recorded at the South Sandwich (SSSZ 1-10) source zone. Maximum and minimum values were not provided from development but visual comparisons between the development cases (shown in figures 11, 12 and 16 of the model report) and the forecast system output were consistent in shape and amplitude for all cases. The Charlotte Amalie reference point used for the forecast model development is the same as what is deployed in the forecast system, so the results can be considered valid for the three cases studied.

Scenario Name	Source Zone	Tsunami Source	α (m)	SIFT Max (cm)	Development Max (cm)	SIFT Min (cm)	Development Min (cm)
ATSZ 38-47*	Atlantic	A38-47, B38-47	25	508.1	493.3	-370.0	-379.4
ATSZ 48-57*	Atlantic	A48-57, B48-57	25	768.7	800.9	-425.9	-463.6
SSSZ 1-10*	South Sandwich	A1-10, B1-10	25	65.6	75.3	-61.5	-86.3

Table 9: Table of maximum and minimum amplitudes at Charlotte Amalie, Virgin Islands warning point for synthetic and historical events tested using SIFT.

*Some difference between the testing results and the results obtained during the model development is due to an update of the propagation database, which resulted in using slightly different synthetic scenarios for development and for testing.

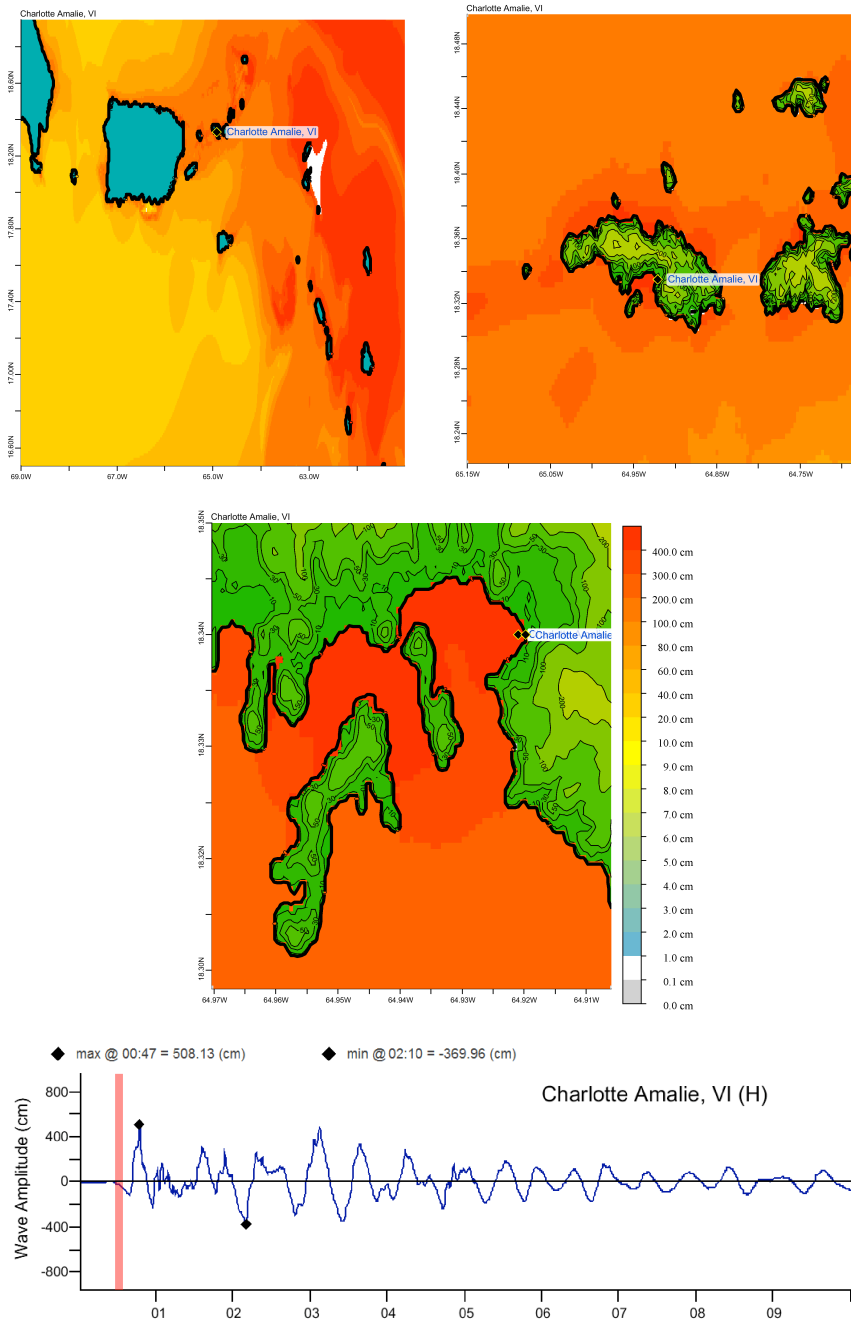


Figure 32: Response of the Charlotte Amalie forecast model to synthetic scenario ATSZ 38-47 (alpha=25). Maximum sea surface elevation for A⁵-grid (top left), B-grid (top right), C-grid (center). Sea surface elevation time series at the C-grid warning point (bottom), to be compared with the red curve in Figure 11, top pane.

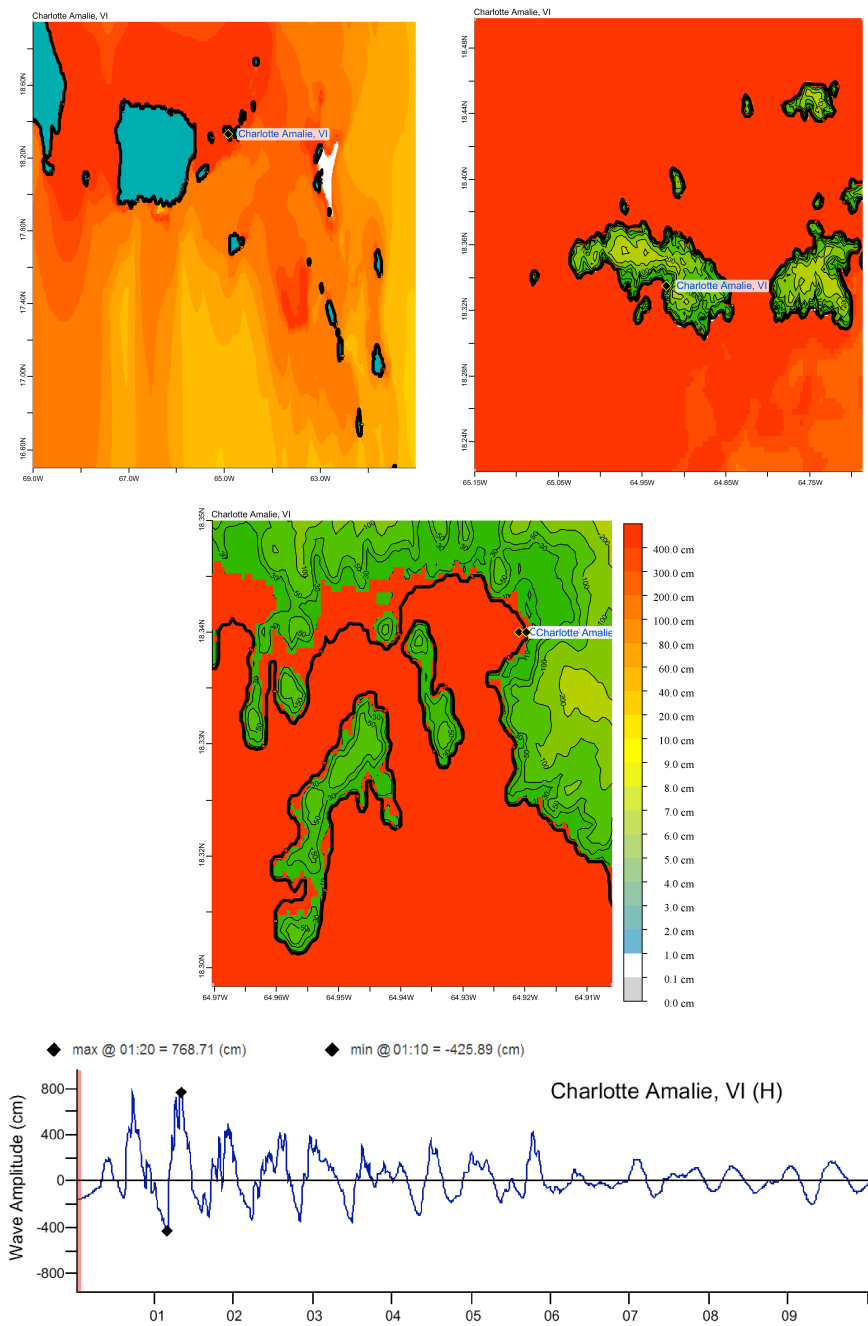


Figure 33: Response of the Charlotte Amalie forecast model to synthetic scenario ATSZ 48-57 (alpha=25). Maximum sea surface elevation for A-grid (top left), B-grid (top right), C-grid (center). Sea surface elevation time series at the C-grid warning point (bottom), to be compared with the red curve in Figure 12, top pane.

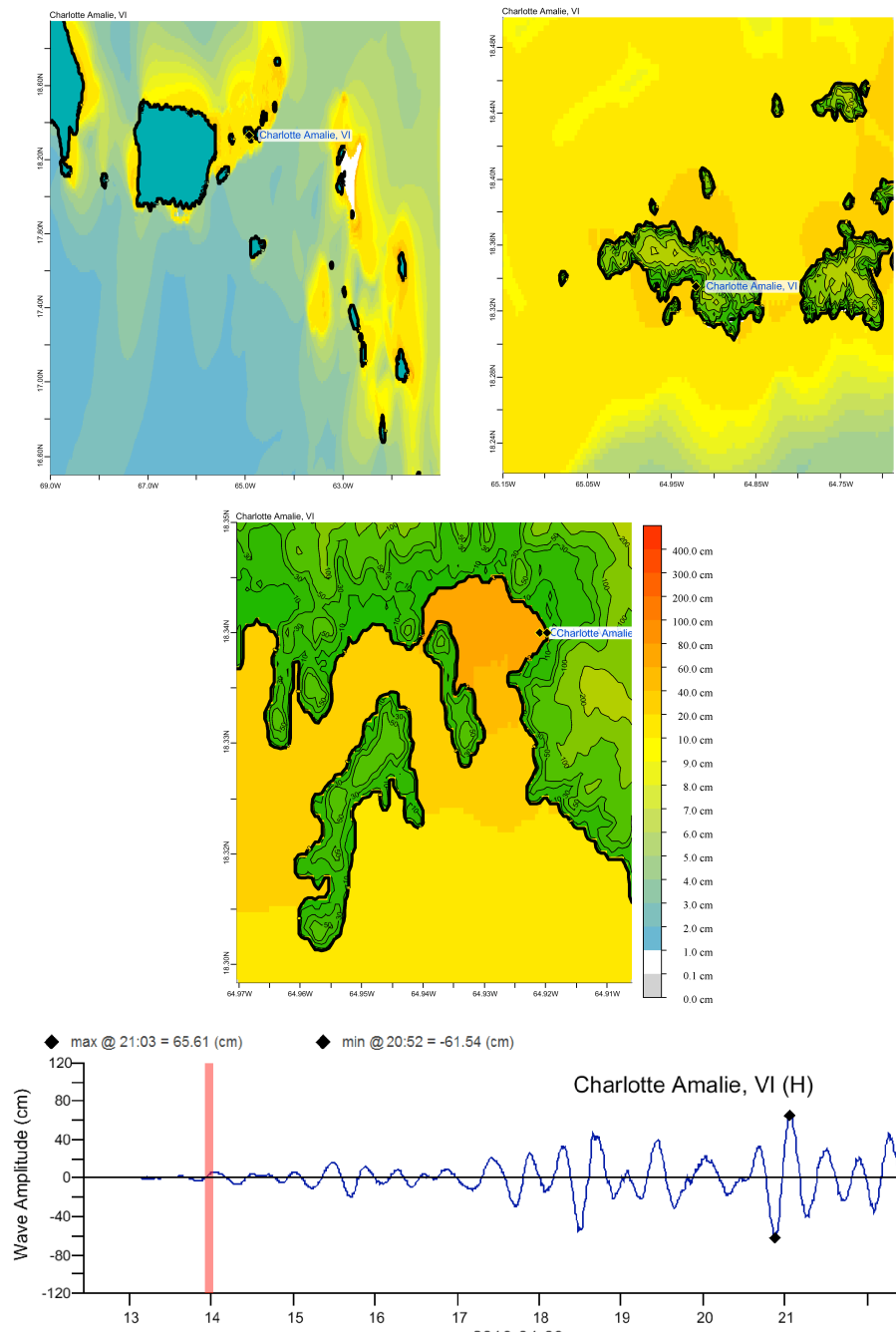


Figure 34: Response of the Charlotte Amalie forecast model to synthetic scenario SSSZ 1-10 (alpha=25). Maximum sea surface elevation for A-grid (top left), B-grid (top right), C-grid (center). Sea surface elevation time series at the C-grid warning point (bottom), to be compared with the red curve in Figure 16, top pane.